ANNUAL REVIEWS

Annual Review of Fluid Mechanics

3D Lagrangian Particle Tracking in Fluid Mechanics

Andreas Schröder[1,2] and Daniel Schanz[1]

[1]Institute of Aerodynamics and Flow Technology, Deutsches Zentrum für Luft- und Raumfahrt (DLR), Göttingen, Germany; email: andreas.schroeder@dlr.de

[2]Institute for Traffic Engineering, Brandenburgisch Technische Universität (BTU) Cottbus–Senftenberg, Cottbus, Germany

Annu. Rev. Fluid Mech. 2023. 55:511–40

First published as a Review in Advance on October 13, 2022

The *Annual Review of Fluid Mechanics* is online at fluid.annualreviews.org

https://doi.org/10.1146/annurev-fluid-031822-041721

Keywords

3D particle tracking velocimetry, iterative particle reconstruction, Shake-The-Box, one- and multipoint statistics, velocity gradient tensor, 3D pressure fields, data assimilation

Abstract

In the past few decades various particle image–based volumetric flow measurement techniques have been developed that have demonstrated their potential in accessing unsteady flow properties quantitatively in various experimental applications in fluid mechanics. In this review, we focus on physical properties and circumstances of 3D particle–based measurements and what knowledge can be used for advancing reconstruction accuracy and spatial and temporal resolution, as well as completeness. The natural candidate for our focus is 3D Lagrangian particle tracking (LPT), which allows for position, velocity, and acceleration to be determined alongside a large number of individual particle tracks in the investigated volume. The advent of the dense 3D LPT technique Shake-The-Box in the past decade has opened further possibilities for characterizing unsteady flows by delivering input data for powerful data assimilation techniques that use Navier–Stokes constraints. As a result, high-resolution Lagrangian and Eulerian data can be obtained, including long particle trajectories embedded in time-resolved 3D velocity and pressure fields.

1. INTRODUCTION

Lagrangian particle tracking (LPT) is a volumetric flow measurement technique capable of following high numbers of tracer particles over extended periods of time, even in highly turbulent scenarios. In this introduction we physically motivate the importance of these and related techniques, introduce the general principle, provide an overview of the historical development, and describe recent advances in postprocessing. In-depth discussions of these topics are provided in Sections 2–4.

Most flows we encounter in everyday life are unsteady, turbulent, and three dimensional (3D). The Reynolds numbers reached in nature, aerodynamics, and in many relevant technical applications are typically far above the onset of turbulence. Human beings are literally immersed in unsteady fluid flow phenomena, from those in our blood vessels and respiratory tracts to flows around and inside various transport vehicles, currents in oceans, atmospheric turbulent boundary layers (TBLs), and mixed thermal convection inside closed rooms. In order to make any technical use of fluid flows, one needs to understand their Lagrangian and Eulerian properties in detail in various applications and situations. The main features of turbulent flows are their dynamic energy transfer mechanism in a cascade from large to increasingly smaller (vortical) flow scales down to dissipation (Richardson 1922) and their increase of spatial and temporal scale separation with Reynolds number as $L/\eta \sim Re_\lambda^{3/4}$ and $T_L/\tau_\eta \sim Re_\lambda^{1/2}$ (Toschi & Bodenschatz 2009; see also the sidebar titled Scales of Turbulent Flows).

Turbulent flow structures can be defined as 3D topologies, either stable or unstable saddle-points or stable or unstable nodes, according to the local velocity gradient tensor (VGT) (Chong et al. 1990), that change their shape and orientation in time while convecting (downstream) with the bulk flow. On the other hand, the flow and its coherent structures themselves can be understood and described as a dynamic composition of an almost infinite number of fluid elements that are moving with the local flow as Lagrangian trajectories and are coupled with neighboring elements by pressure gradients and viscosity. In a Lagrangian frame of reference, these fluid elements are entering and exiting more persistent Eulerian coherent flow structures, thereby keeping them alive or leading to their final decay. Therefore, flow topologies can be defined either in a Eulerian (laboratory) reference system, for example, by the invariants Q and R of the VGT (for incompressible flows), or from a Lagrangian perspective as Lagrangian coherent structures (LCS) (Haller 2015) moving with the fluid elements. Nevertheless, both reference systems allow the same flow to be described, as the Lagrangian and Eulerian velocity vectors are identical for each time step.

Fluid flow dynamics follow physical laws describing their momentum exchange and mass conservation by a set of equations, which were first discovered by Navier and Stokes. These governing laws are nonlinear partial differential equations and, nowadays, allow numerical methods to

SCALES OF TURBULENT FLOWS

The Reynolds number Re expresses the ratio of inertial to viscous forces in the flow by, for example, $Re_\lambda = U \cdot \lambda/\nu$, while U is the flow velocity, λ is the Taylor micro-length scale, and ν is the kinematic viscosity. For $Re \gg 1$, the flow is typically turbulent and consists of a broad range of flow scales. The integral length scale and timescale are denoted L and T_L, respectively, which are measures for the largest and most persistent flow structures. The Kolmogorov length scale and timescale, η and τ_η, respectively indicate the smallest flow structures and shortest timescales that lead to dissipation into heat. Therefore, a flow measurement technique that allows for a wide range of flow scales to be captured is desired. For the technical capabilities of Lagrangian particle tracking, it is of importance that the spatial scale separation, L/η, grows faster with Re_λ than the temporal one, T_L/τ_η.

predict flows and their features by computer simulations, such as for aerodynamical design purposes. At high Reynolds numbers, the resolution requirements in space and time and the nonlinearity of the flow physics involved pose many problems for numerical codes, regarding either the available computer resources or the validity and applicability of established turbulence models or scaling laws (Mani & Dorgan 2023). A very high degree of computational effort is already needed for predicting turbulent flows at moderate Reynolds numbers by direct numerical simulations (DNS). Today, even with modern high-performance computing resources, converged DNS results (e.g., for the flow around a small passenger aircraft) cannot be provided at all and will most probably not be reachable within the next couple of decades. Therefore, (advanced) computational fluid dynamics code developments that use turbulence or subgrid-scale models to solve their closure problem [large eddy simulations, (unsteady) Reynolds averaged Navier–Stokes (NS) equations, etc.] require spatially (and temporally) well-resolved experimental validation data at high Reynolds numbers, preferably in full volumes around various model geometries. High-quality velocity vector fields (instantaneous and mean with Reynolds stresses) enable the tuning of numerical parameters and the adaptation or further development of various turbulence models. Promising fields that will be closely linked to velocity, acceleration, and pressure data from 3D LPT measurements in the near future include data-driven turbulence models (Duraisamy et al. 2019) and the exploration of universal constants (Viggiano et al. 2021) or turbulent transport properties in inhomogeneous turbulence from Lagrangian statistics.

Particle image velocimetry (PIV): flow measurement method for obtaining 2D fields of velocity vectors by cross-correlating subsequent images of tracer particles

Particle tracking velocimetry (PTV): LPT method that applies triangulation and subsequent connection of particle positions gained from successive images

1.1. Particle Image–Based Velocimetry

During the past decades a tremendous increase of flow field information has been gained from experimental investigations applying image-based measurement techniques. Particle image–based methods visualize the flow using clouds of small tracer particles that are illuminated and observed by one or more cameras (complementary or alternative to existing probe techniques). For experiments in unsteady and turbulent flows, nonintrusive volumetric and time-resolved measurement techniques, determining all three components of the velocity (and acceleration) vectors at many points instantaneously, are highly desired. Consequently, in recent years particle image velocimetry (PIV) techniques have been extended from 2D to 3D and from two-pulse snapshot modes to temporal resolution (Adrian & Westerweel 2011, Raffel et al. 2018, Beresh 2021). Various volumetric (and time-resolved) PIV and particle tracking velocimetry (PTV) techniques and their capabilities have already been presented in dedicated papers. For single (or stereo) camera views, scanning PIV has been proposed by, for example, Gray et al. (1991) and Brücker (1997); holographic PIV techniques have been presented by Hinsch (2002), Katz & Sheng (2010), and others; coded aperture PIV was first introduced by Willert & Gharib (1992); defocusing PIV was described by Pereira et al. (2000); structured-light PIV was described by, e.g., Aguirre-Pablo et al. (2019); and light field or plenoptic PIV was described by Fahringer et al. (2015) and others. Applications of single-camera 3D PTV for microfluidics include astigmatism (Cierpka et al. 2010) and holographic PTV (Choi et al. 2012). Single-view 3D PIV and PTV techniques can operate with less optical access, but due to the limited aperture, the reconstructed particle position uncertainty in depth direction (the direction parallel to the main viewing direction of the camera) is much larger (typically by a factor greater than 3) compared to the in-plane uncertainties. Multicamera methods rely on several camera projections, allowing similar position and velocity uncertainties in all three directions in space when appropriate projection angles are applied (ideally an angle of 90° is used between the two outermost cameras—the "aperture" of the camera system).

Tomographic PIV (Tomo-PIV), which was introduced by Elsinga et al. (2006) and further developed by Wieneke (2008), Atkinson & Soria (2009), and Novara et al. (2010), significantly

enhanced the spatial resolution of volumetric velocimetry. Therefore, Tomo-PIV rapidly evolved to become the most commonly used and robust 3D flow measurement technique in the decade following its first publication. It enables flow field estimates to be delivered on regular 3D velocity vector grids via iterative local cross-correlation schemes with relatively high spatial resolution based on, typically, four to six camera projections and at particle image densities around $N_I = 0.05$ particles per pixel (ppp). Furthermore, by using many camera projections one can increase the number of truly reconstructed particles per time step while reducing the so-called ghost particle fraction (Elsinga et al. 2006), which holds true as well for particle-based reconstruction schemes for 3D LPT. For all 3D reconstruction techniques, N_I determines the possible spatial resolution inside the investigated flow for a given depth of the measurement volume; however, the reconstruction difficulty increases with N_I. The maximum value of N_I at which a method can reliably reconstruct true particles while not creating too many ghost particles typically determines its performance. Novel machine learning (ML) approaches are promising methods for increasing the range of N_I-values for Tomo-PIV techniques (Gao et al. 2021). A further increase of spatial resolution or particles per volume (ppv) has been achieved by a scanning Tomo-PIV setup in a turbulent low-speed flow (Lawson & Dawson 2014). However, for all cross-correlation-based PIV techniques, a spatial low-pass filter modulation of the velocity gradients inside the measured flow has to be accepted because only a group of particle images (typically four to ten) located inside a 2D or 3D correlation window [e.g., 32^2 px (pixels) or 32^3 voxels] enables a robust estimation of the position of the local displacement vector peak. Furthermore, acceleration vector fields are not directly accessible by this method. Consequently, a measurement technique that enables individual tracer particles to be followed volumetrically and at high densities in time is more suited to bridge the scattered measurement data, including position, velocity, and acceleration, along reconstructed particle trajectories to the governing NS equations.

Particle image density, N_I: measure to describe the density of particle image peaks on a camera image; expressed in particles per pixel (ppp)

Ghost particle: falsely reconstructed 3D particle (position) that does not exist in the originally imaged particle cloud

Peak: image of a single particle on a camera, typically a (distorted) Gaussian with a diameter of 2–3 pixels

Line-of-sight (LOS): the viewing path through the measurement region of a given camera image coordinate, as given by the calibration

$\overline{\text{px}}$: normalized length of a camera pixel, scaled by the average magnification; it is thereby a universal measure for comparing 3D imaging systems

1.2. Particle Tracking Methods

In contrast to PIV methods, particle tracking methods have been developed with 3D PTV schemes that enable relatively sparse particle track reconstructions (e.g., Nishino et al. 1989, Maas et al. 1993, Malik et al. 1993, Guezennec et al. 1994, Virant & Dracos 1997, Ouellette et al. 2006, Machicoane et al. 2019, Dabiri & Pecora 2020) at particle image densities between ∼0.005 and 0.02 ppp. Increased particle track densities in the measurement volume can be achieved with scanning 3D PTV techniques (Hoyer et al. 2005, Kozul et al. 2019), reaching higher ppv values for relatively low flow velocities. Nowadays, state-of-the-art 3D LPT techniques can reach high particle image densities of ∼0.05–0.2 ppp using the Shake-The-Box (STB) method (Schanz et al. 2016, Jahn et al. 2021, Leclaire et al. 2021, Sciacchitano et al. 2021b).

Figure 1 depicts the general working principle of 3D particle tracking experiments: First, particle images of (illuminated) passive tracers inside the flow are taken simultaneously from several camera projections (typically three to six) for each time step. Then, particle image peaks are detected on each camera and the lines-of-sight (LOS) of each peak are virtually elongated into the measurement volume according to the 3D camera calibration. When LOS of detected particle image peaks on several cameras intersect below an allowed triangulation error (∼1 $\overline{\text{px}}$), a true 3D particle position can be assumed. Using all detected peaks on the different cameras, one can reconstruct clouds of 3D particle positions for each time step. A tracking approach is then applied in a second step that aims at always finding the identical imaged particle along the corresponding timeline of 3D particle reconstructions in order to build up long 3D particle trajectories. The actual implementations of the different LPT steps can be performed with varying levels of sophistication and are discussed in Sections 2 and 4.

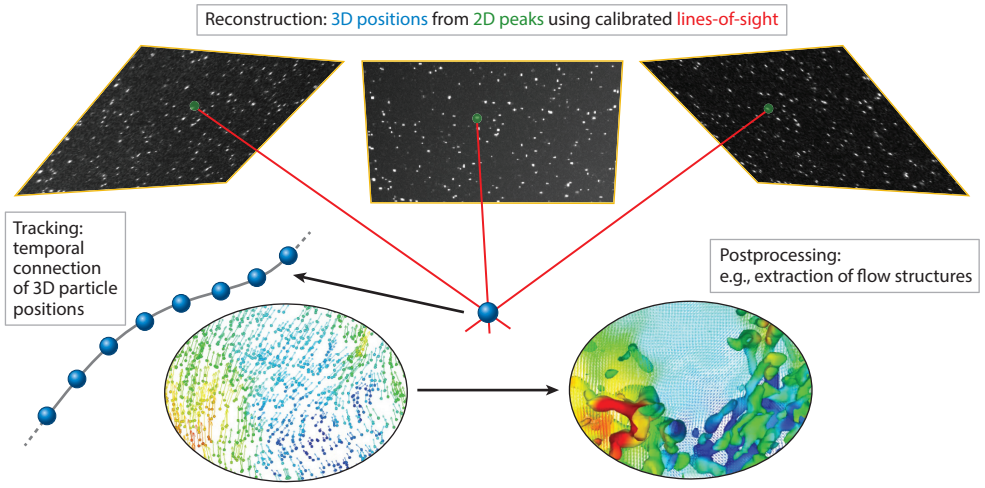

Figure 1

The basic steps of a Lagrangian particle tracking experiment. 2D particle images (peaks) are identified on all camera images for a certain time step (*green dots*) and then used to determine 3D positions (*blue dots*) using (iterative) triangulation procedures (*red lines*). The particle clouds from several time steps can be connected to tracks under certain constraints. Velocity and acceleration of the trajectories yield several properties via postprocessing (e.g., flow structures) by applying regularized interpolation (data assimilation) to all particles tracked at a certain time step.

Figure 2 shows a specific application of LPT in a large and densely seeded Rayleigh–Bénard convection cell. The key aspects of the setup are a pulsed volumetric illumination and a multicamera setup consisting of at least three cameras and capable of temporally resolving the flow. Here, the STB algorithm (see Section 3.1) was used to instantaneously track up to 560,000 tracers over long periods of time from the images obtained from six cameras (Bosbach et al. 2021, Godbersen et al. 2021).

Here we would like to suggest using the name "3D LPT" for volumetric measurements of individual particle trajectories (following, e.g., Ouellette et al. 2006) because the achievable measures along individual particle paths are manifold, including position, velocity, acceleration (material derivative), and (sometimes even) jerk, as well as their Lagrangian properties. All of these are important for the fluid mechanical characterization of the investigated flow and are valuable inputs for high-resolution postprocessing approaches using bin-averaging for one- and multipoint statistics, data assimilation (DA), ML, and integration [e.g., pressure from LPT (Rival & van Oudheusden 2017, van Gent et al. 2017)]. The velocity, as might be suggested by the term "PTV," is not the only important outcome.

Tomo-PIV and 3D LPT/PTV techniques, as well as various similar volumetric velocimetry techniques for fluid flows, have been extensively presented and discussed in recent reviews (e.g., Scarano 2013, Westerweel et al. 2013, Discetti & Coletti 2018, Machicoane et al. 2019) and textbooks (Schröder & Willert 2008, Adrian & Westerweel 2011, Raffel et al. 2018, Dabiri & Pecora 2020). Furthermore, with the recent development of high-speed lasers and cameras, the range of flow velocities in which time-resolved velocity field information can be gained via PIV and LPT has been widened significantly in spatial and temporal resolution (Beresh 2021).

In all various volumetric flow measurement techniques, the achievable dynamic spatial range (DSR) (see Adrian 1997) for sampling any (turbulent) flow field is mainly restricted by the resolution of the used camera sensor and the reachable volumetric particle density, which limit the

Data assimilation (DA): the process of combining measurement data (e.g., particle position, velocity, acceleration) and theory (Navier–Stokes equations) for maximizing resolution

Dynamic spatial range (DSR): the ratio of the extent of a measurement region and the smallest resolvable scale

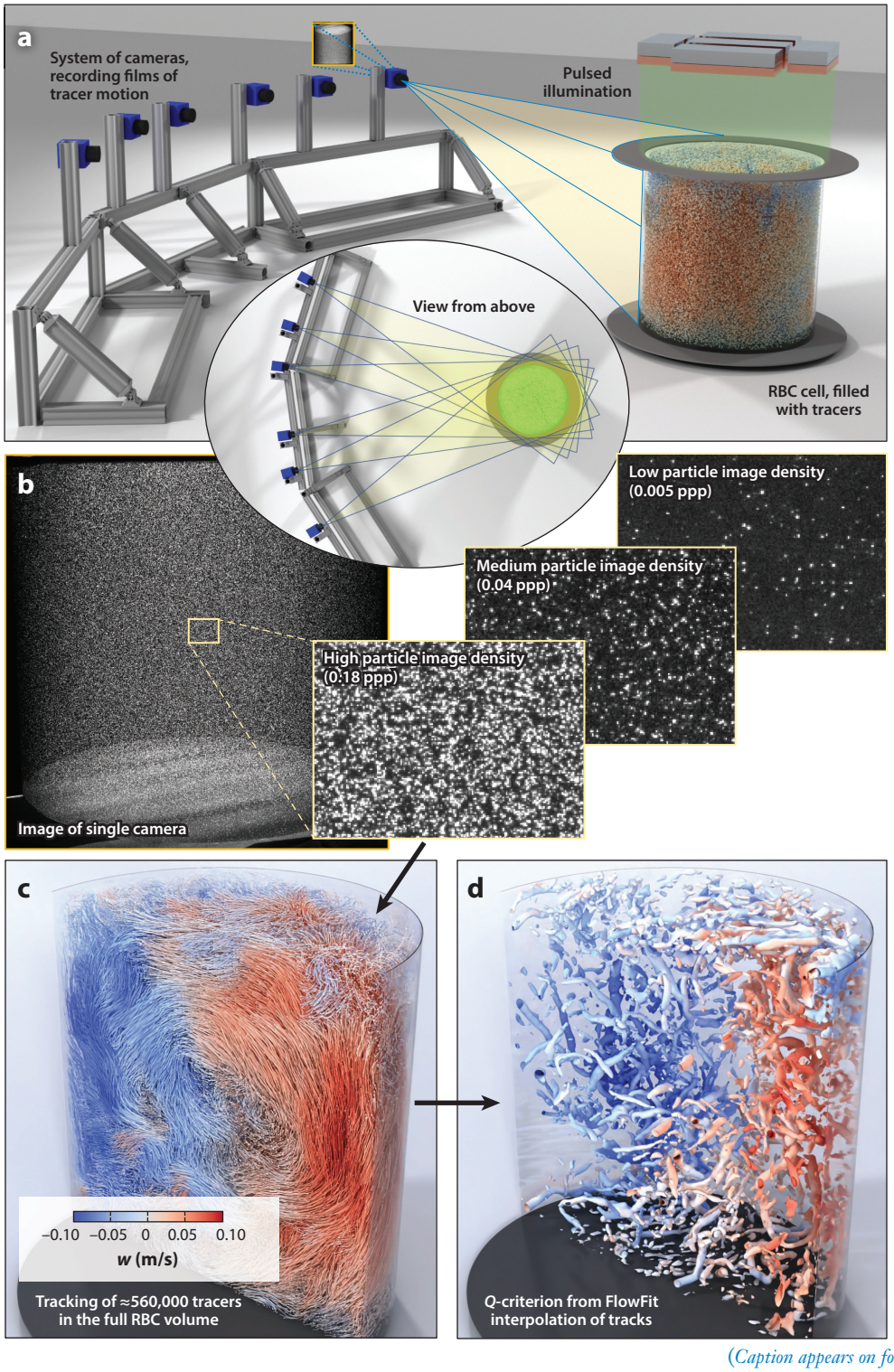

(*Caption appears on following page*)

Figure 2 (*Figure appears on preceding page*)

(*a*) Exemplary setup of a Lagrangian particle tracking (LPT) experiment, consisting of a Rayleigh–Bénard convection (RBC) cell 1.1 m in height with tracer particles (here, helium-filled soap bubbles) illuminated by a pulsed light source (here, from above by arrays of high-power LEDs (light-emitting diodes) shining through a transparent water-cooled top plate). The illuminated tracers are recorded in a time-resolved fashion by a system of cameras, all imaging the same (illuminated) volume. (*b*) Actual image from one camera of the experiment, showing bubbles inside the cell and the illuminated heated floor. The insets show examples at several particles per pixel (ppp) concentrations. (*c*) LPT was performed on the high-density images using the Shake-The-Box method. (*d*) Flow structures can be visualized by applying FlowFit data assimilation to the tracked particle field in panel *c*. Panels adapted from Godbersen et al. (2020) (CC BY-NC 4.0; **https://doi.org/10.1103/APS.DFD.2020.GFM.V0074**).

instantaneous sampling of the largest and smallest achievable flow structures, respectively. The latter is directly related to N_I and the depth of the investigated volume. Therefore, if flow dynamics and repetition rates of cameras and illumination allow, 3D scanning methods can achieve relatively high volumetric particle densities (and DSR values) and do not suffer (like many other techniques) from both the reduction of scattered particle light due to small camera lens apertures and the expansion of the available (laser) light for full volumetric illumination.

On the other hand, the dynamic velocity range (DVR) (Adrian 1997) and dynamic acceleration range (DAR) (Schanz et al. 2016) are strongly linked to the reconstructed particle position accuracy and the temporal sampling along the (exploitable) particle trajectories. To enhance DSR and DVR of particle-based measurements, the need for a "completely new approach" has already been proclaimed (Westerweel et al. 2013, p. 409). In general, multi-illumination or time-resolved imaging strategies of tracer particles inside flows enable higher accuracies than can be achieved with two-pulse strategies when determining temporal derivatives of the particle trajectory. All three characteristic values, DSR, DVR, and DAR, can be maximized in a 3D LPT experiment by exploiting the knowledge of the physical (fluid mechanical and optical) properties of the individual tracer particles and their imaging. Applying this physical knowledge for an enhanced 3D particle reconstruction and tracking scheme was the path followed by the STB development in the past decade. High position accuracies of reconstructed particles require well-sampled particle images (~2 px in diameter, no pixel-locking) at high signal-to-noise ratio (SNR), as the discretized gray values of particle images contain the particles' position information. Then, the applied 3D reconstruction scheme should aim at a strong reduction of ghost particles in order to keep the distributed image intensity at the true particles' positions for enhancing their position accuracy. Finally, having obtained such high positional accuracies, accurate temporal derivatives along fitted tracks, like velocity and acceleration, are only available at sufficiently high sampling frequencies. With respect to extreme but rare acceleration events inside turbulent flows, it has been proposed that one samples at least 40 times faster than the Kolmogorov timescales, τ_η, in order to avoid respective tracking and truncation errors (Lawson et al. 2018). However, hardware restrictions do not always allow for such high illumination and imaging frequencies. In Section 3.2 below the temporal sampling problem for high-acceleration (and -jerk) events is addressed again in the context of an advanced prediction and correction STB scheme.

1.3. Advanced 3D Particle Tracking and Data Assimilation Techniques

Dynamic velocity range (DVR): the ratio of the highest measured velocity and the minimum measurable velocity (typically limited by noise)

The STB technique is an advanced 3D LPT method that combines the triangulation-based advanced iterative particle reconstruction (IPR) technique (Wieneke 2012, Jahn et al. 2021) with the exploitation of the temporal and spatial coherence of Lagrangian particle tracks in the investigated flow. STB enables the processing of particle image densities up to $N_I = 0.2$ ppp under good experimental conditions with an almost complete suppression of ghost particles. Subsequently, the dense scattered particle tracks are temporally filtered (Gesemann et al. 2016, Gesemann 2021) for estimating position, velocity, and acceleration (material derivative), which can be used in a second

step as input for DA approaches using NS constraints, delivering the full time-resolved 3D velocity gradient tensor and pressure fields (e.g., Gesemann et al. 2016, Schneiders & Scarano 2016, Jeon 2021). Using only solenoidal constraints applied to dense LPT data, in case D of the Fourth International PIV Challenge in 2014, the first DA schemes have already shown better spatial and temporal resolution of the reconstructed volumetric flow field than advanced Tomo-PIV techniques (see Kähler et al. 2016). A further benchmark test of the 3D pressure field reconstruction capabilities of various pressure from PIV and LPT approaches also showed strong benefits in using dense LPT data, delivering velocity and acceleration vector fields as input for DA schemes that apply fully nonlinear NS constraints (see van Gent et al. 2017). Current developments aim at maximizing the achievable flow information from single flow experiments at high particle image densities by applying (combined) 3D LPT, DA, and ML (Brunton et al. 2020) approaches. However, in many high-speed flow experiments, full temporal resolution for particle image–based volumetric velocimetry is still not possible. Here, multipulse and multi-illumination techniques for Tomo-PIV (Lynch & Scarano 2014, Schröder et al. 2013) and LPT (Novara et al. 2016b, 2019) have been developed that can capture volumetric velocity fields at high spatial resolution, as well as DVR (see **Figure 5**) (e.g., van Gent et al. 2017).

The scattered nature of the individually tracked particles provides a great advantage over other related measurement techniques such as PIV. Instead of a fixed regular grid of convolution windows whose size imposes a low-pass filtering effect on resolvable flow structures and gradients, the particle track positions are distributed homogeneously and provide local point measurements of fluid elements when using particles with diameters below the smallest scales of the investigated flows, such as the Kolmogorov length scale $d_p < \eta$, and at low Stokes numbers $St \ll 1$. This can be exploited in Eulerian ensemble averaging using spatial binning to realize very fine (subpixel) resolutions since the bin size is primarily limited by the amount of available data and the fitted position accuracy. This allows for a direct trade-off between bin size and convergence of the underlying statistics (Schröder et al. 2015). One particularity of LPT is that the position, velocity, and acceleration of a particle can be determined not only at each measured timestep but also, inherent to the postprocessing, continuously along the full reconstructed track (Godbersen & Schröder 2021). The position accuracy of a measured particle path along the filtered track is typically in the range of 0.1 $\overline{\text{px}}$. In the context of characterizing the results of evaluation methods, the normalized pixel unit $\overline{\text{px}}$ has evolved as a universal measure of length due to its transferability between different measurements or synthetic test cases.

There have been attempts to quantify the uncertainty of LPT measurements on a spectral level (Gesemann 2021), on a single–particle trajectory level (Janke & Michaelis 2021), and as a full framework that tries to account for various noise and bias sources (Bhattacharya & Vlachos 2020). For DA, methods like track benchmarking (Schneiders & Sciacchitano 2017) and synthetic benchmark tests can be used (van Gent et al. 2017, Sciacchitano et al. 2021a).

By now, LPT constitutes a measurement tool that allows for accurate 3D flow measurements in a multitude of flows at high spatial and temporal resolution. In the following, we highlight the main steps of its evolution, discuss potential obstacles, and present ideas and developments for further advances.

2. PREREQUISITES FOR DENSE 3D LAGRANGIAN PARTICLE TRACKING

2.1. 3D Particle Tracking Velocimetry

The first approaches to characterizing an underlying flow by following the trajectories of tracer particles used manual tracking of singular particles and date back to the beginning to middle of the

twentieth century (Nayler & Frazer 1917, Chiu & Rib 1956). Agüí & Jimenez (1987) provided a review and assessment of PTV methods mainly established before the advent of digital cameras, as well as their interpolation strategies. The systematic extension to the joint 3D tracking of particles in larger numbers took place in the early 1990s with developments in digital 3D PTV by Nishino et al. (1989) and especially Maas et al. (1993) and Malik et al. (1993). These algorithms function by triangulating 3D positions from projections of the particle field on multiple cameras, followed by a secondary tracking step connecting physically reasonable appearances in successive triangulated particle clouds (see **Figure 1**).

Optical transfer function (OTF): the shape of the particle image (typically Gaussian), which may differ depending on particle position due to optical effects

The triangulation process presumes an accurate calibration of the viewing direction for each camera, for example, using a Tsai or a simple pinhole camera model (Raffel et al. 2018). Peaks are identified on all cameras and 3D locations are determined by applying epipolar geometry with an allowed triangulation error ε. The triangulation process is performed for each time step independently. Trajectories are then extracted by successively examining the reconstructions for particles that minimize a certain cost function for each already identified track. The cost functions can be a simple nearest-neighbor approach, more elaborate methods that seek to minimize the acceleration over several past and future time steps (see Malik et al. 1993, Ouellette et al. 2006, Xu 2008), or probabilistic frameworks (e.g., Herzog et al. 2021).

A multitude of methods for particle image identification, positioning, tracking, and postprocessing have been developed in the scope of 3D PTV (Dabiri & Pecora 2020). The technique has been successfully applied in many research areas; one of the most prominent applications was turbulent flows to investigate, for example, acceleration statistics (La Porta et al. 2001), velocity statistics (Xu 2008) or vorticity dynamics (Lüthi et al. 2005) by examining particle tracks over very long examination times (Shnapp et al. 2019). The downside of the approach is the triangulation process's limited particle image density and the increase of ambiguities within the tracking process with increasing particle number. Therefore, the applicable particle image density N_I rarely exceeded 0.005 ppp (see **Figure 2*b***).

2.2. Advances in Calibration Accuracy

The determination of an accurate calibration for all cameras is a key aspect in all volumetric measurement techniques. A geometrical calibration is typically performed using either a 3D calibration target or a 2D target translated to at least two parallel positions, yielding an accuracy of the order of 1 $\overline{\text{px}}$. On the PTV side this accuracy was regarded as sufficient, mainly because the low particle image densities allow one to treat ε in a relatively flexible manner.

This changed with the introduction of Tomo-PIV in 2006 (Elsinga et al. 2006, Scarano 2013). Tomo-PIV reconstructs particles as intensity blob distributions in large arrays of voxels ($\sim 10^9$) for each time step and subsequently applies local 3D cross-correlation schemes of two (or more) subsequent intensity distributions to determine a regular grid of (low-pass-filtered) volumetric velocity vectors. The multiplicative nature of the MART (multiplicative algebraic reconstruction technique) algorithm used for tomographic reconstruction (Herman & Lent 1976, Atkinson & Soria 2009) requires that the pixels corresponding to an intersection point in object space on all cameras be nonzero. A decalibration results in a shift of the pixel matrix and would therefore create a different 3D intensity blob distribution, with more energy distributed to initially empty places (ghost particles), reduced intensity at the true particle locations, and distortions of their 3D shape. The insight that sub-pixel-accurate calibrations are required led to the development of the volume self-calibration (VSC) method; see the sidebar titled Volume Self-Calibration.

Building upon VSC, a calibration procedure of the optical transfer function (OTF) (Schanz et al. 2013a) of the particles in several subvolumes was developed, accounting for the often-varying

VOLUME SELF-CALIBRATION

A calibration of a 3D camera system using a calibration target is limited by the number of markers on the target and the accuracy with which these are positioned and detected. Furthermore, calibration errors can be introduced by vibrations, physical interaction, or thermal effects.

The VSC method (Wieneke 2008, 2018) uses measurement images themselves to correct and refine the initial target calibration. A triangulation process is applied on sparse images (low ppp values) to determine preliminary 3D positions, possibly allowing a large triangulation error to counteract the initial decalibrations. The triangulated particles are then back-projected onto the different cameras and the differences of the back-projection to the original particle peak are determined, giving an indication of how much each camera is decalibrated in relation to the others. Averaging these differences over many particles yields disparity vectors, which are used to correct the initial 2D-3D mapping functions. By iterating the process, the calibration errors can typically be corrected below 0.1 $\overline{\text{px}}$. Recently, further calibration methods have been developed to account for distortions beyond the order of the applied calibration model (Schanz et al. 2019, Michaelis et al. 2021).

imaging conditions across the measurement volume between the different cameras and within a single camera frame. This allows for a precise matching of the reprojected and the original particle image, thereby increasing accuracy and reducing the residual. Note that VSC and OTF calibration both are particle based in nature and directly use particle imaging properties. Not only does this make the gained information ready for use in particle position–based reconstruction schemes, like IPR and STB, but it also means that the necessary algorithmic structures (like peak detection and triangulation) can be directly used, thereby reducing the development effort.

2.3. Toward High-Density Particle Reconstruction

PTV had shown that a direct knowledge of particle positions is highly desirable—only that this method was severely limited by the usable particle image density. Combining the stability of tomographic reconstruction and the benefits of particle tracking, Tomo-PTV attempts to identify 3D particle peaks within tomographically reconstructed volumes and track those over two or more frames (Schröder et al. 2011, Doh et al. 2012, Novara & Scarano 2013, Fuchs et al. 2016, Bross et al. 2019, Cornic et al. 2020). The usable particle densities can indeed be elevated compared to PTV (up to around 0.05 ppp); however, the position accuracy is limited by the 3D peak detection and processing times, and memory demands are high due to the large voxel space.

A major step in reverting to pure particle tracking was the development of IPR by Wieneke (2012). This procedure represents an iterative approach to triangulation with intermediate particle position optimization, as discussed in more depth below. The underlying idea is that particles that could not be found by an initial triangulation should be easier to identify once the reconstruction problem is already partly solved. For a particle to be successfully triangulated, a peak needs to be identified for the corresponding particle image in all cameras at an accuracy within the allowed triangulation error ε. Such an identification can be inhibited by image noise, image distortions, or, most importantly, an overlap with the images of other particles. In such cases the detection of all concerned particle peaks is compromised or even completely prevented. This problem becomes very common once high particle image densities are targeted. At $N_I = 0.1$ ppp most particle images overlap with another particle image (Cierpka et al. 2013). With rising N_I, common peak-finding algorithms (e.g., Ouellette et al. 2006) increasingly underestimate the particle number and the position accuracy declines. Above a certain limit of N_I, the number of peaks found using a classical peak detector remains nearly constant, despite the additional particle images (Michaelis et al.

Reprojected image: projection of 3D points onto a virtual camera using the calibration and drawing the OTF around the projection point

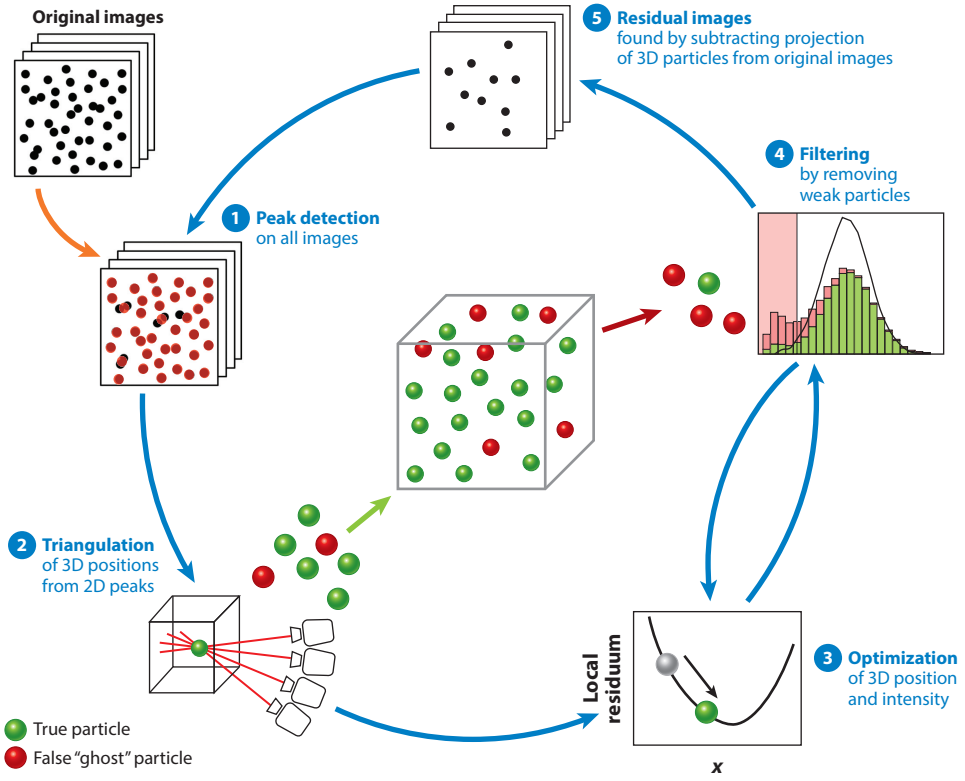

Figure 3

Iterative particle reconstruction scheme, consisting of multiple steps running iteratively in outer and inner loops: (❶) peak detection on original or residual images, (❷) triangulation of 3D positions, (❸) 3D position and intensity optimization ("shaking"), (❹) filtering of 3D positions by intensity (steps ❸ and ❹ are processed iteratively in an inner loop), and (❺) subtraction of reprojected 3D positions from original particle images. The residual image is used as input for another iteration of all five steps in order to amend particle positions not yet found in further outer loops. Figure adapted from Jahn et al. (2021) (CC BY 4.0).

2010). From this point on, the found peaks represent local maxima of overlapping particle clusters, instead of single particles. These considerations show that simple triangulation is bound to fail even at moderate particle image densities. IPR shifts this limitation using several approaches. The general scheme, consisting of an inner and an outer loop, is depicted in **Figure 3**.

The process starts with a normal 3D triangulation using peaks identified on the original images. This step is followed by a particle position optimization [see the sidebar titled Position Optimization (Shaking the Particles)]. The particle intensity is optimized alongside the position. Particles, whose intensity falls below a threshold, are deleted as they are assumed to be false reconstructions (ghost particles). The optimization and filtering process is itself applied iteratively (N_{SHAKE} executions of the inner shaking loop), with intermediate updates to the residual image. By this approach, the particles are implicitly informed of the state of other particles with which they share an overlapped image in one or more cameras. Therefore, the initially local method (each particle is optimized independently) yields a quasi-global solution after some optimization iterations.

Once position and intensity have been optimized for the current particle distribution, the remaining particles are used to create residual images. These should be void of the already known particles so that the remaining peaks can be better identified, as overlap situations have been

POSITION OPTIMIZATION (SHAKING THE PARTICLES)

The 3D position of reconstructed (triangulated) particles typically exhibits a certain error due to limited peak detection accuracy, noise, and image overlap. However, an optimization can be attempted that modifies the triangulated 3D positions, such that the reprojected image of each particle best matches the local image patch on all cameras simultaneously.

For most methods, the position is shifted iteratively following the gradient descent of a cost function R, which is defined by the difference of the measured image and the reprojection (the sum of the local residuals). Due to the iterative shifting, while approaching the minimum of R, this process is often referred to as shaking the particles. This gradient decent can be determined either numerically (Wieneke 2012) or analytically (Jahn et al. 2021). A different approach by Yang & Heitz (2021) uses a kernel optimization to deduct the optimal particle position. Thus, the combined information from all cameras imaging a certain particle is used to correct the inaccuracies introduced by the peak detection on the individual cameras.

This process also acts as a corrector scheme of the prediction step in the STB algorithm (see Section 3.2).

(partly) resolved. Having found the peaks on the residual image, another triangulation is performed, the newly found 3D particles are added to the already known cloud, and the particles are again treated by iterative position/intensity optimization and filtering. The outer loop is repeated for N_{IPR} iterations. For low-noise synthetic data, applying many iterations of outer and inner loops can help to converge to a full solution at very high position accuracy (<0.01 $\overline{\mathrm{px}}$); for noisy (experimental) data, both N_{IPR} and N_{SHAKE} can be kept reasonably low (three to five iterations), as the position accuracy is in any case dominated by the image noise. For an accurate position optimization and realistic creation of the projected image it is evident that the demands on both the geometrical calibration and the OTF calibration are high.

The requirement that a peak be found on all cameras can be difficult to achieve. Therefore, IPR can apply triangulations, where particles are also accepted if a peak is not present in one or more cameras, thereby greatly increasing the number of correctly triangulated particles at the cost of an increased creation of ghost particles. The scheme was applied by Wieneke (2012), who found an accurate reconstruction of noise-free synthetic images at particle image densities up to $N_I = 0.05$ ppp.

Recently, Jahn et al. (2021) showed an advanced IPR that further extends the working range by several considerations. Firstly, the peaks found on the first two considered cameras upon triangulation determine the examined 3D coordinates. Therefore, a particle cannot be found if its peak is missed in either of these. The use of several permutations of the camera order when triangulating prevents this effect. Secondly, the intensity of a particle is determined as an average of all cameras during the optimization process. However, ghost particles are often only supported by bright peaks on a single or few cameras. Therefore, ignoring the N_{Ci} (locally) brightest cameras for the intensity determination significantly reduces the intensity (and thereby the number) of ghost particles, while having only an insignificant impact on the true particles. Thirdly, ghost particle creation grows exponentially with the allowed triangulation error ε. By gradually increasing ε with each triangulation, one can reconstruct well-defined true particles at the beginning; larger values of ε are only reached in a stage when the low number of still-present peaks reduces the probability of creating a ghost particle.

With these measures, IPR is able to fully reconstruct particle distributions from noise-free synthetic images up to $N_I = 0.14$ ppp (Jahn et al. 2021). Introducing moderate image noise and particle intensity variations only slightly worsens these results, apart from the positional error that

rises to ~0.1 $\overline{\text{px}}$. Heavy image noise and strong intensity variations inhibit the reconstruction of all true particles; however, ghost levels still remain low at moderate N_I (Jahn et al. 2021, Sciacchitano et al. 2021b).

Helium-filled soap bubbles (HFSB): tracers, reflecting light, used for large-scale measurements in air; often used with LED illumination

2.4. From Synthetic to Experimental Data

It has to be noted that the conditions encountered in real-life experiments are typically quite different from those produced by synthetic test data. Often the scattering behavior of the tracer particles is not regular for several directions and in time due to polydisperse size distributions, Mie scattering lobes, nonspherical particles, particle surface properties, and speckles from coherent light sources. Certain particles scatter more light in one camera than in others, depending on their size, shape, rotation state, and position (Raffel et al. 2018). While the position-resolved relative intensity of the particle images on different cameras is known from the OTF calibration in an average sense, single particles can deviate considerably from this calibration. In such a case the reconstruction problem is not uniquely solvable. For the same reasons, a single particle can vary in intensity over time while moving through the illuminated volume.

The intensities of overlapping particle images might not sum up perfectly on each camera due to several effects. Occultation of two or more particles can partly block light coming from far particles. When using laser illumination, the light scattered on two particles in a proximity smaller than the coherence length of the laser can interfere along the LOS toward a camera, causing a speckle pattern instead of the sum of two Gaussians. These effects can severely aggravate peak detection and the resolution of overlap situations. On the other hand, very good results in these aspects can be achieved by using helium-filled soap bubbles (HFSB) in air or fluorescent particles in water as tracers and incoherent light sources such as pulsed LEDs (light-emitting diodes) for illumination. Inhomogeneities in the illumination stemming from the laser beam profile or other sources of diffraction patterns (knife-edges, dust on lenses, etc.) can lead to intensity variation of the scattered light along a moving particle.

Non-Gaussian particle imaging is often caused by astigmatism due to properties of imaging lenses or viewing nonperpendicularly through interfaces of different indices of refraction. Aperture effects (edges or model parts along the LOS) can lead to severe particle image distortions and depth-of-focus limitations to blurring of particles. Background intensity or light reflections at model surfaces of the particle images require appropriate preprocessing steps, such as subtraction of a minimum image or more advanced spectral-based (Mendez et al. 2017) or ratio-cut methods (Wang et al. 2020). Viewing through a contaminated medium (e.g., not illuminated seeding particles, dirt, algae) can cause the image quality to be heavily deteriorated, with only limited chances of recovery by image-processing schemes.

In general, particle imaging conditions for LPT experiments should be organized such that the scattered particle light is of sufficient SNR and of similar intensity for all camera viewing directions (e.g., the same scattering angle with respect to the (laser) light propagation) and consistent over time for all moving particles inside the illuminated volume. Pixel-locking, astigmatism, and blurring of particle images should be avoided by adjusting focus and aperture and using prisms. Therefore, the physical properties of the light scattering (e.g., Mie scattering, reflection), the light source itself, the image background, and the particle and its surface have to be considered thoroughly.

3. SEIZING TEMPORAL INFORMATION

The effects discussed in the previous section can lead to a significant reduction in reconstruction performance of single–time step experimental data compared to synthetic data for all reconstruction algorithms. However, for each experiment, a certain amount of additional information is

available through the temporal evolution of the particle field, recorded at two (double-pulse), few (multipulse), or many (time-resolved) successive time steps. Each recorded time step represents a (slightly) novel view on the particle distribution, enabling the detection of previously hidden information. Combining this information can improve the reconstruction of the full data set.

The connection of particle reconstructions in classical PTV applications represents a filtering step, separating the particles found on physically reasonable trajectories from the ones that appear more randomly in the volume. Thereby, the reconstructions are purged from probable ghost particles; however, correctly reconstructed particles might also be discarded if the triangulation failed in neighboring time steps. The filter is applied as a postprocessing of the reconstruction, without feedback.

A first attempt to improve the reconstruction via information from other time steps was developed within the Tomo-PIV framework as motion-tracking-enhanced MART (Novara et al. 2010). Here, the correlated velocity result of two or more time steps was used to mutually dewarp the reconstructed voxel spaces, leading to a suppression of ghost particle intensities. Later a time-marching version of the method was developed, which was shown to work up to $N_I = 0.2$ ppp (Lynch & Scarano 2015). Recently, Lasinger et al. (2020) published an integrated approach that combines a joint IPR process of two time steps and the regularized deduction of a connecting flow field using a global energy minimization. The process works reliably on high-density particle images, albeit currently only for two frames.

In 2013, inspired by the introduction of IPR two years earlier and the results of Tomo-PTV, the STB method was developed for time-resolved data (Schanz et al. 2013b, 2016), which not only incorporated temporal information into the reconstruction process but also introduced a reversal of the logic chain: Instead of first reconstructing a particle position distribution for each time step separately, in which matches for known tracks are searched as a second step, the algorithm preinitializes a to-be-reconstructed time step with all particles for which a track is already known. The precise positioning within the current time step is achieved by a predictor/corrector scheme. Only at this point are the remaining unknown particles reconstructed, whose number is typically low compared to the number of already tracked and reliably predicted particles. Two simple physical conditions are used here: (*a*) An existing real particle, moving inside an illuminated volume, does not disappear, and (*b*) the particle path is sufficiently smooth according to the underlying fluid mechanics and temporal resolution. Therefore, its existence in each following time step can be presupposed and quite accurately predicted, and this will be manifested by the images. The STB tracking scheme does not need to learn, or be informed of, the underlying flow physics, as it intrinsically makes use of them without any preknowledge. The debatable constraint of sufficient smoothness of the particle tracks is addressed in Section 3.2, with a focus on rare high-acceleration events in turbulent flows. With an increasing number of known particles, the creation of ghost particles is increasingly suppressed. The algorithm converges to a self-stabilizing solution where mostly only particles entering the measurement domain need to be identified, thereby drastically enhancing the usable seeding density and reducing the computational effort. For achieving a good (or sufficient) spatial and temporal resolution in a 3D LPT experiment, one needs to consider DSR, DVR, and DAR by setting an appropriate size of the measurement volume for a given camera resolution, as well as a sufficiently high seeding concentration and acquisition frequency for the flow under investigation.

3.1. Outline of Time-Resolved Shake-The-Box

The working principle of the STB technique is outlined in **Figure 4** and further described below. At the beginning of a time series, no prior information is available; therefore, the method starts with an initialization phase akin to a standard tracking evaluation (**Figure 4**). The first N_{init} time

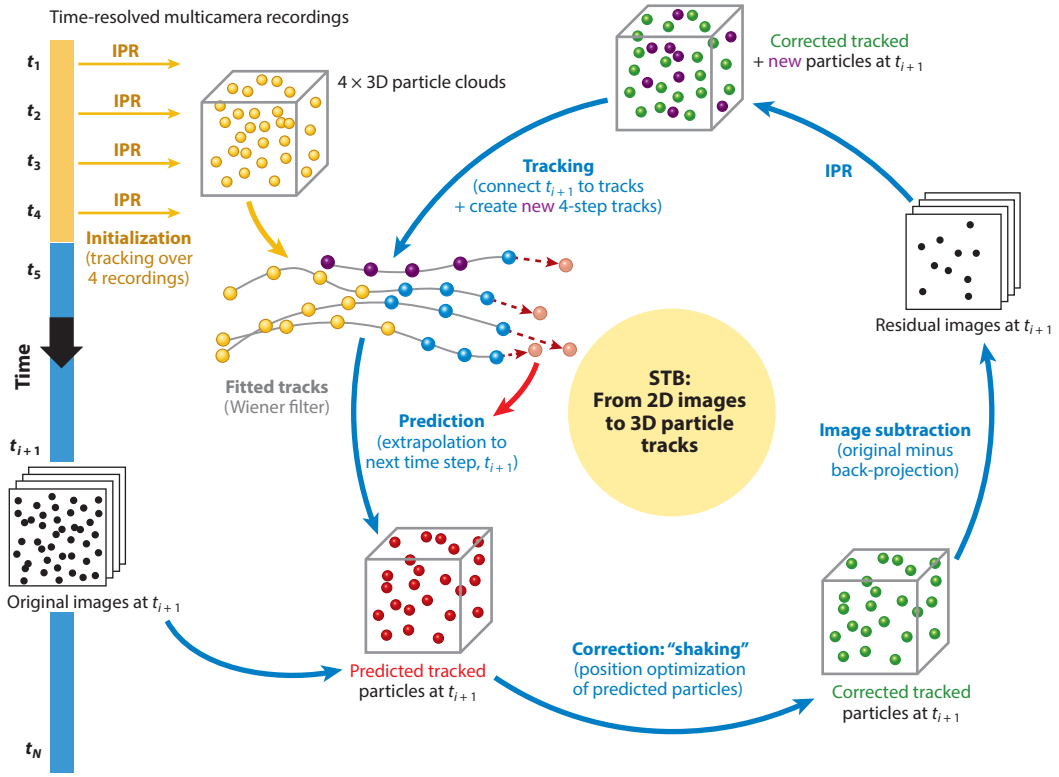

Figure 4

Shake-The-Box (STB) processing. The STB scheme is initialized with iterative particle reconstruction (IPR) processing of four subsequent time steps (t_1 to t_4) from multicamera particle images and subsequent temporal connection to 3D particle tracks (*yellow*). Next, the particle position of each track is predicted for the next time step (t_{i+1}) by extrapolating suitable temporal fitting functions (*red*). Then, 3D position and intensity optimizations are applied by the shaking approach and residual images are calculated (*green*). An IPR process is applied to the residual images, yielding new 3D positions (*purple*); corrected predictions and new 3D positions are used to finally elongate the existing tracks to the current time step (*blue*) and identify new tracks from the yet untracked particles of the last four time steps (*purple*, akin to the initialization).

steps (typically $N_{\text{init}} = 4$) are reconstructed using (advanced) IPR. Within these particle clouds, connected sequences of particle positions (track candidates) are identified. To this end, several methods of varying fidelity are available (Ouellette et al. 2006). The track candidates are then confirmed as identified tracks using a maximum-acceleration constraint and the condition that each reconstructed particle can only be part of one track. A prior sorting of the track candidates based on the average acceleration increases the stability. Further discriminators between true and false tracks can be the inclusion of the surrounding flow field (Schanz et al. 2016, Khojasteh et al. 2021) or particle-space correlations (Novara et al. 2016a).

With the steps above, tracks of N_{init} length have been identified that fall within the physical boundaries of the experiment. These tracks are then used to preinitialize the particle field at time $t_{N_{\text{init}}+1}$ by predicting the position of the tracked particles at this time step using, for example, a polynomial fit, a Savitzky–Golay filter (Savitzky & Golay 1964), or a predictive Wiener filter (Wiener 1949). In any case, the choice of the prediction filter should reflect the expected accelerations and the position noise level. Due to acceleration, noise, overlapping particle images, and other experimental factors, the predictions will exhibit certain deviations from the true position,

which need to be corrected. For this purpose, the position-optimization scheme applied within the IPR scheme can be reused. While the positional errors encountered within IPR are usually on the order of the allowed triangulation error, the range of position deviation can be noticeably higher when predicting a particle position. As discussed in Section 3.2, the prediction of the vast majority of particles can still be shifted to the correct position. Once the already tracked particles are placed correctly, particles that are not yet tracked or newly entering the domain are then detected. For this, IPR is applied on residual images (created by subtracting the projections of the predicted and corrected particles from the original recordings) that are significantly less populated, thereby simplifying the reconstruction of the still missing particles. From these newly reconstructed particles at $t_{N_{\text{init}}+1}$ and the still-untracked particles of t_2 to $t_{N_{\text{init}}}$, additional tracks of length N_{init} are extracted (**Figure 4**) and added to the set of tracks being predicted at $t_{N_{\text{init}}+2}$. The search for new tracks can be aided by velocity information of already tracked neighboring particles. This scheme is reiterated for all available steps in the time series. The number of tracked particles steadily grows (convergence phase) until it reaches a state where mostly only particles that are entering the measurement domain have to be identified. Nearly all other particles are correctly placed by the corrector/predictor scheme prior to any reconstruction efforts (converged phase). This scheme of tracking before reconstruction constitutes a reversal of the PTV strategy and defines the stability of the tracking process as a time-marching self-optimization.

After reaching the end of the time series, a second pass can be performed, operating backward in time. At each time step, the particles tracked in the first pass are used to preinitialize the IPR object. A track that was starting at time step t_n in the first pass is predicted at t_{n-1} and followed backward in time until leaving the measuring domain (the entering point in forward time). The second pass complements tracks that were not immediately identified and fills up the time steps at the beginning of the time series, where the tracking system was still converging (see Schanz et al. 2016, figure 13, or Huhn et al. 2017, figure 10). Often it is not necessary to perform IPR during the second pass—a pure prediction and correction of ending (originally starting) tracks is sufficient.

As an example, **Figure 2*c*** shows tracking results of STB evaluations of a measurement on a cylindrical Rayleigh–Bénard convection cell 1.1 m in height and diameter, filled with HFSB. Only half of the measured volume is displayed. Up to 560,000 bubbles are instantaneously tracked. The local particle image density in the middle of the field of view is $N_I = 0.18$ ppp (the average over the full image is $N_I = 0.12$ ppp). Processing of each time step takes below 45 s on a Ryzen 3950X 16-core processor.

It is noteworthy that the parameters for the initial identification of tracks can typically be set conservatively. A reliable rejection of false tracks is thereby achieved, possibly missing the ones in highly accelerated regions. As a full time series is available, these particles will eventually be transported into calmer regions and picked up by the tracking process there. The high-acceleration event will then be captured in the second pass by following the particle backward in time.

Since 2020 an open source code project inspired by the ideas of the STB scheme has been available; it is described for shadow graphic LPT by Tan et al. (2020).

3.2. Prediction Errors and Their Correction

Individual particle trajectories exhibiting high accelerations pose an obstacle to the tracking process. If the track is not yet known, an identification at the time instant of the acceleration may be inhibited by the maximum-acceleration constraint. If, on the other hand, the particle is already tracked, the prediction of the new location might show a strong deviation from the real position once the acceleration event is reached (this should be the prevailing case in a converged

tracking system). It has been shown recently (Schanz et al. 2022) that position-optimization methods based on a gradient descent (Fletcher & Powell 1963, Jahn et al. 2021) can reliably correct particle position errors up to 2.3 $\overline{\text{px}}$ for the two in-plane directions (orthogonal to the cameras' main viewing direction). Even larger errors can be corrected in the depth direction, depending on the angle of the camera setup. At typical recording rates—limiting the particle shift to below 10 $\overline{\text{px}}$—only extreme events would exhibit such large accelerations so that the particle cannot be recovered by the position optimization. However, the misprediction of the position can be amplified by noise, overlapping particle images, nonoptimized prediction, or a low temporal sampling of the flow. In order to handle such conditions, Schanz et al. (2022) introduced the variable space step (VS) method, an approach to correct large, but rare, prediction errors by using an iterative grid search for a small subset of particles. Using this method, even mispredictions in the range of 10 $\overline{\text{px}}$ can be corrected with high probability. In a sample case, in a synthetic turbulent flow with an average particle shift per time step of ∼20 $\overline{\text{px}}$, using noisy image data at $N_I = 0.1$ ppp, one could correct ∼95.3% of all particle predictions by pure position optimization, while ∼99.5% of particle predictions could be corrected by additionally applying VS. This allows for reliable particle tracking in turbulent flows even at relatively low temporal sampling. In such cases, however, a slight underestimation of extreme events due to truncation may still occur.

Other correction schemes that do not rely upon a gradient determination have also been developed. Yang & Heitz (2021) introduced a variational approach to the prediction step that involves performing multiple predictions on perturbations of the past positions, followed by a position determination via a learned function. They found an increased tracking of highly accelerated particles compared to a basic implementation of STB. A quantitative study of its correction abilities has yet to be performed.

In addition to increasing the working range of the position correction, the prediction step can also be improved. Incorporating prior knowledge—like averages of previous evaluations or numerical simulations—could inform the tracking process of expected flow structures (e.g., statistically stationary accelerations in the vicinity of an object). The 3D flow field could be extrapolated using the currently tracked particles to predict the presence of vortices in the path of a particle and accordingly modify the prediction point. This could be performed on a particle level [e.g., extending the ideas of Khojasteh et al. (2021)] or even using NS-regularized DA methods (Gesemann et al. 2016, Schneiders & Scarano 2016, Jeon 2021) with reliable advection schemes toward the interrogated time step, which would constitute a further incorporation of the flow physics (in addition to the continuity of the particle trajectories) in the reconstruction/tracking process and, in turn, would progressively enhance the DA quality.

3.3. Tracking in Highly Dynamic Flows

High-density particle tracking in flows with a high DVR (e.g., jet flows) exhibits some peculiarities. The acquisition rate has to be chosen such that the fastest particles can be reliably tracked. However, slowly moving particles in the entrainment regions can pose a problem for the tracking algorithm due to long-lasting situations of particle image overlap in several camera projections and a quasi-static generation of ghost particles. One solution to these issues is to introduce an iterative tracking approach that consists of several passes (forward and backward in time) at decreasing time separations [variable time step STB (VT-STB) (Schanz et al. 2021)]. This way, a tracking of particles at their respective optimal temporal sampling can be achieved. VT-STB can be seen as complementing the VS method discussed in the previous section. While VS deals with high-acceleration events, VT treats the effects of slow flow regions or bulk motion with low accelerations.

3.4. Multipulse Particle Tracking

The previous sections have worked out the benefits of a time-resolved series of measurements for reconstruction and accuracy. However, such measurements cannot always be performed, mostly due to hardware limitations when the flow of interest is too fast for the available cameras or illumination. In such cases, the typical approach is to revert to double-frame cameras, which can sample the flow twice with very low interframe time (less than 200 ns, depending on the cameras). As mentioned in Sections 2.3 and 3, several high-density two-frame particle tracking methods have been developed (Fuchs et al. 2016, Cornic et al. 2020, Lasinger et al. 2020, Novara et al. 2022), exploiting the advantages of particle-based measurements in high-speed flows [e.g., the creation of highly resolved profiles (Kähler et al. 2012)]. Limitations arise from the missing temporal information. The partner search (i.e., connecting two 3D positions of the same particle at two time steps) can be ambiguous. Additionally, the position and velocity errors are elevated due to the lack of a temporal fit, and acceleration is not available at all (Kähler et al. 2016, Sciacchitano et al. 2021a). As discussed by Westerweel et al. (2013), an extension of the typical two-pulse setup to more pulses would greatly enhance the abilities of PIV and LPT measurements in high-speed flows. Such an extension was introduced by Novara et al. (2016a) as Multi-Pulse-STB, working with two separate camera and illumination systems, separated by polarization. Later, the experimental setup was simplified by an evaluation strategy, working with two double-illuminated exposures on a single two-pulse system (Novara et al. 2019). The concept of multiple illuminations on a single image can even be used in time-resolved measurements to increase the temporal resolution (Schanz et al. 2019). The setup and results of a multipulse experiment are given in **Figure 5**. The Multi-Pulse-STB method was successfully applied in boundary layer flows (Novara et al. 2019), on a laminar wing at 80 m/s (Geisler et al. 2016), and on jet flows at Mach 0.31 and 0.59 (Sellappan et al. 2020) and at Mach 0.506 and 0.845 (Manovski et al. 2021). Increased laser pulse intensities for volumetric, multipulse illumination of small tracer particles can be provided as well by pulse-burst laser systems (see, e.g., Lynch & Wagner 2022).

3.5. Temporal Filtering

When the process of particle tracking is finished, the tracks consist of raw particle positions for all time steps. A temporal filter is used to increase the positional accuracy and to extract the Lagrangian velocity and acceleration (see **Figures 2*c*** and **6**, as well as the left and middle of **Supplemental Video 1**). To this end, various methods are applicable. A polynomial fit of second or third order can be applied, with the possibility of tuning the filter strength to the experiment via the length of the used kernel. This kernel can even be dynamically adapted to the current state of the particle (Janke & Michaelis 2021). Another approach is the use of a (cubic) B-spline curve whose filter strength can be calibrated to the noise conditions by deducting a crossover frequency from the position amplitude spectrum, which also yields the average position accuracy (Gesemann et al. 2016, Gesemann 2021). The method can be tuned to be equivalent to an optimal Wiener filter. As a rule of thumb, the positional errors can be nearly halved by applying a well-calibrated filter.

Supplemental Material >

4. POSTPROCESSING OF LAGRANGIAN DATA

LPT methods simultaneously yield long Lagrangian trajectories for a multitude of particles and a discrete field of velocity and acceleration information at the particle locations for each time step, and even in between them, given the continuous filtering. This allows one to go beyond the diffraction limitation of particle imaging for two-point statistics (Godbersen & Schröder 2020, Hammond & Meng 2021). A broad field of research to benefit from such enhanced 3D LPT methods is particle-laden turbulence, especially when collisions need to be considered

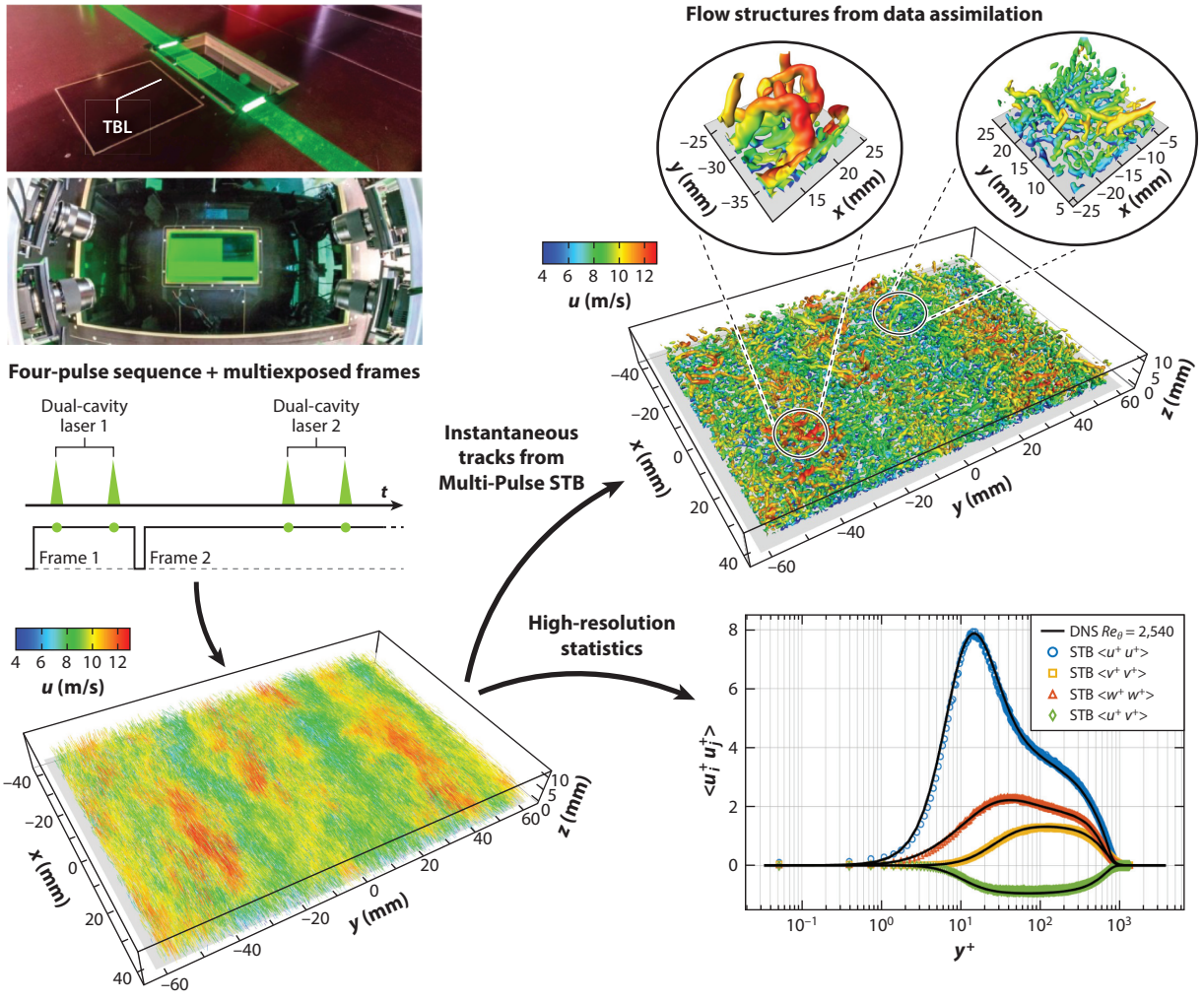

Figure 5

Exemplary measurement using Multi-Pulse STB: A TBL flow with a micrometer-sized droplet seeding is illuminated by two double-pulse lasers ($80 \times 120 \times 10$ mm^3) and observed by eight double-frame cameras, illuminating each frame twice. From each image pair, approximately 95,000 particles are tracked. This data can be used, for example, by data assimilation for flow structure identification or by bin-averaging methods to determine high-resolution profiles of velocity and Reynolds stresses. Figure adapted from Novara et al. (2019), with permission from Springer; copyright 2019 Springer-Verlag. Abbreviations: DNS, direct numerical simulation; STB, Shake-The-Box; TBL, turbulent boundary layer.

(Brandt & Coletti 2022). Inertial particles (Ebrahimian et al. 2019) and slip over superhydrophobic surfaces (Abu Rowin & Ghaemi 2019) in turbulent boundary layers have been investigated using STB. Besides the creation of highly resolved Lagrangian and Eulerian statistics, the tracking data may be used in various ways, as described below.

4.1. Bin Averaging

Advanced binning procedures can produce a 3D array of one-, two-, and multipoint statistics of the flow (mean values, Reynolds stresses, two-point correlations, structure functions, etc.) at very high spatial resolution, down to subpixel accuracies. According to Reynolds (triple)

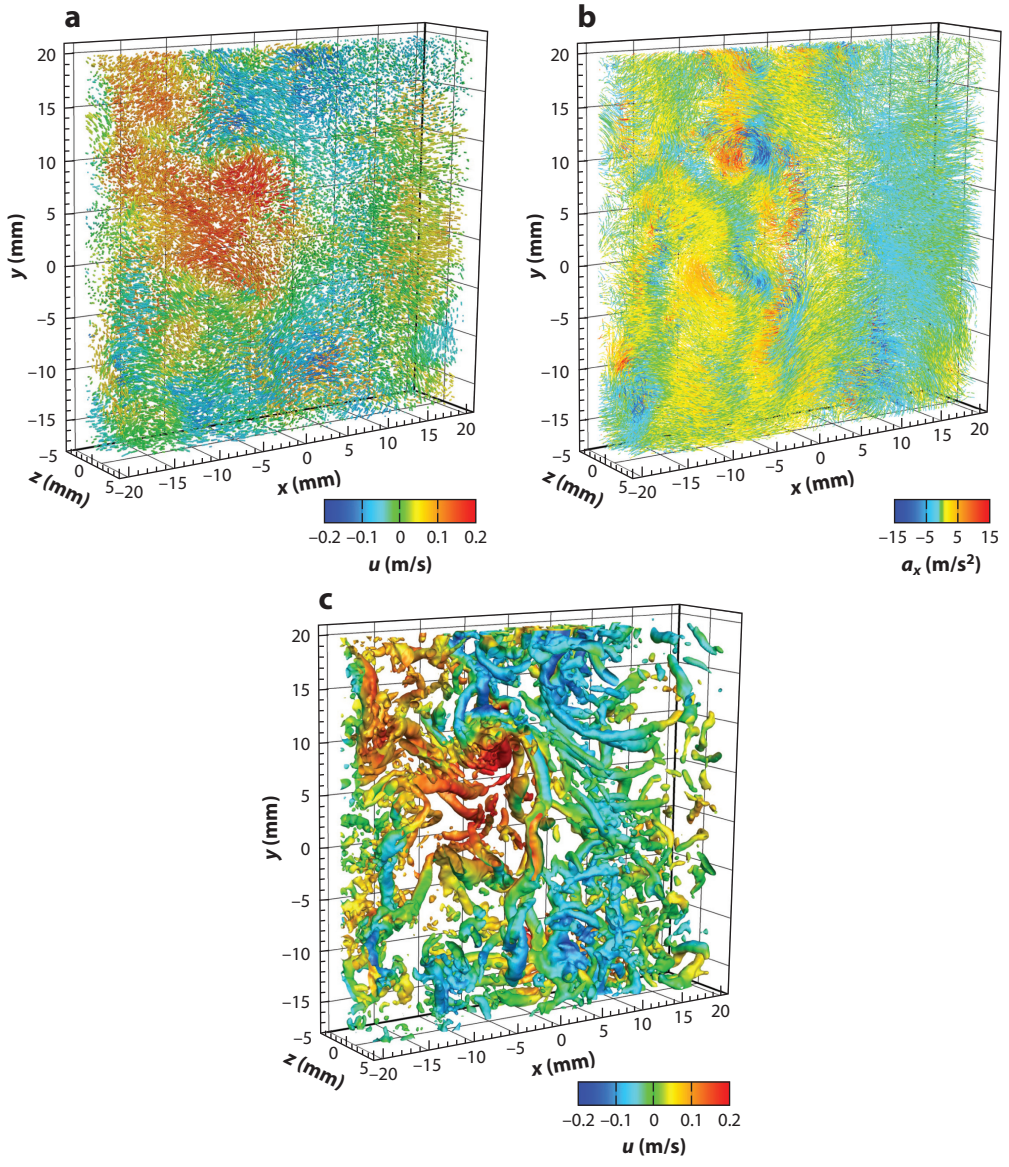

Figure 6

Lagrangian particle tracking measurement in homogeneous turbulence at $Re_\lambda = 270$ in a von Kármán water flow between two counter-rotating propellers (Schröder et al. 2022). (*a*) Approximately 65,000 particles visualized at five consecutive time steps as spheres, colored by *x*-velocity. (*b*) The same flow situation, here with 30 time steps, connected by velocity vectors and colored by *x*-acceleration (a_x). (*c*) Flow structures identified via FlowFit data assimilation of the particle cloud at the central time step, given by an isosurface of the *Q*-criterion ($Q = 2{,}500/\mathrm{s}^2$).

decomposition, $u = \bar{u}(+\tilde{u}) + u'$, the statistical flow quantities are the mean $\bar{u}$ (periodic $\tilde{u}$) and fluctuation u' components of all three velocity vector components. The respective Reynolds stress tensor $\overline{u_i' u_j'}$ and higher-order statistics are further measures for characterizing unsteady and turbulent flows. Profiles of these quantities can be determined by dividing the measurement region into

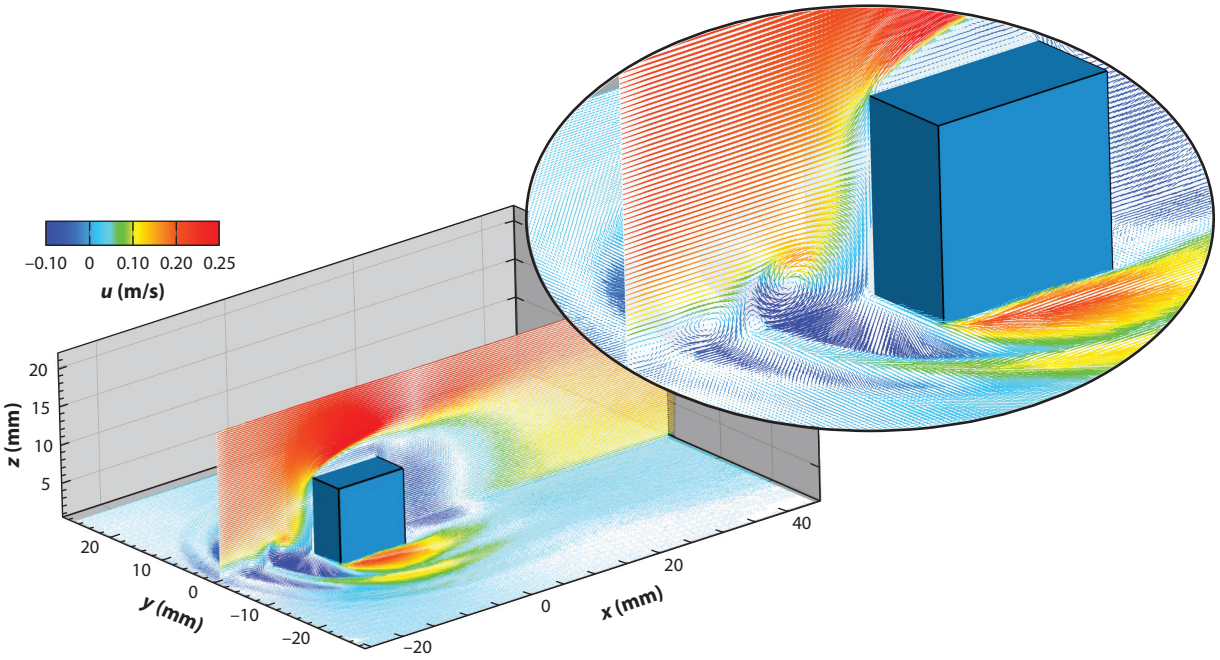

Figure 7

3D bin averaging of the flow around a cube mounted on a surface and submerged in a laminar boundary layer with a flow speed of $U = 0.2$ m/s and a bin size of $0.25 \times 0.25 \times 0.25$ mm^3 (see Schröder et al. 2020).

small subregions (bins) and averaging the properties of all particles located within each of these bins over all measurements available. Depending on the flow and the volume, the profiles can be 1D, 2D, or 3D. **Figure 7** shows a 3D-averaged profile of the flow around a surface-mounted cube, while **Figure 5** displays a 1D profile of Reynolds stresses of a TBL with a resolution of 14.5 μm (1/3 of a viscous unit). The usable size of the bins scales inversely with the number of measurements: The more data that are available, the finer the resolution can be (in contrast to PIV, which is always limited to the correlation window size). Important for the reliability of the statistics is a local convergence study and a precise uncertainty quantification. Recently, a versatile functional binning procedure has been introduced that optimizes the convergence speed of 3D LPT one-point and multipoint statistics by using the continuous track and uncertainty information (instead of sampling the particle only at each measured time step) (Godbersen & Schröder 2020, Godbersen & Schröder 2021). Further measures to increase the spatial resolution have been integrated into the functional approach, such as arbitrarily shaped bins (Raiola et al. 2020) and weights, allowing for adaptation to mean flow gradients (Agüera et al. 2016).

4.2. Data Assimilation for Spatial Interpolation

Representing flow data on a regular grid or in a continuous functional way within a Eulerian frame of reference is desirable for many established processing methods (e.g., for flow structure identification and pressure determination). The availability of Lagrangian velocity and acceleration allows for interpolations that go beyond a simple averaging approach. In the last couple of years, techniques for DA schemes have been established for single- and multi-timestep LPT results using solenoidal constraints or a full incompressible NS regularization. For the latter, velocity and acceleration (material derivative or left side of the NS momentum equation) are used

as input values. Such methods include FlowFit (Gesemann et al. 2016) and vortex-in-cell (VIC) approaches [VIC+ (Schneiders & Scarano 2016), VIC# (Jeon et al. 2018, Jeon 2021), and VIC-TSA (Scarano et al. 2022)]. These DA schemes provide a continuous functional representation of the assimilated velocity vector field without additional spatial filtering, on the basis of (truncated) 3D radial basis functions or third-order B-splines. Analytical derivatives can be computed for the full time-resolved velocity gradient tensor $A_{ij}(t)$ for an arbitrary grid, and 3D pressure fields are implicitly integrated by solving the related Poisson equation and imposing constraints from the incompressible NS equations using nonlinear optimization solvers [e.g., L-BFGS (limited-memory Broyden–Fletcher–Goldfarb–Shanno) (Nocedal 1980; see also van Gent et al. 2017, Huhn et al. 2018)]. In their review on the development of load estimation techniques, Rival & van Oudheusden (2017) explicitly proposed that LPT+DA will become the new standard for instantaneous 3D pressure reconstruction and stated its importance for future measurements of unsteady flows. Examples of DA applied to LPT data can be found in **Figures 2*d***, **5**, and ***6c***, as well as in **Supplemental Video 1** (right panel).

Di(2-ethylhexyl) sebacate (DEHS): a liquid used for the generation of aerosol particles, often used for laser-based flow measurements in air

Supplemental Material >

5. LARGE-SCALE VOLUMETRIC MEASUREMENTS

For a long time during the development of PTV and Tomo-PIV, volumetric investigations remained limited to relatively small volumes. High-speed lasers were used to illuminate DEHS [di(2-ethylhexyl) sebacate] droplets (~1 μm in diameter) in air or suitable tracers in water (e.g., polyamide particles up to 100 μm in diameter, depending on the scales to be resolved). Especially in air, the small tracers restricted the volumes that could be illuminated to a few cubic centimeters. Two developments changed this: the steady progress in the development of LEDs, allowing researchers to build scalable pulsed illumination arrays (Stasicki et al. 2017), and the introduction of submillimeter HFSB tracer particles in air (Bosbach et al. 2009). The light reflected on the ~300-μm-diameter bubbles is orders of magnitude more intense than the light scattered on small oil droplets. At the same time, density matching ensures a high flow-tracing fidelity (Scarano et al. 2015). With laser illumination, the applicable volume size for high-speed investigations grows to several liters (Scarano et al. 2015); for LED illumination, the volume is mostly limited by the number of available LEDs. First attempts by Kühn et al. (2011) used Tomo-PIV in a convection cell with 55 liters of measured volume. The imaging properties of the (noncoherent) light reflected on the bubbles proved to be very favorable for particle tracking methods. Time-resolved investigations of an impinging jet (Huhn et al. 2018) and a turbulent boundary layer (Schanz et al. 2019) have also been performed. The latter reached a volume size of 450 liters. When investigating slow flows (e.g., driven by temperature gradients), one can use illumination times of several milliseconds, further increasing the achievable volume size. A thermal plume has been captured in a volume of 550 liters (Huhn et al. 2017), and the Rayleigh–Bénard flow depicted in **Figure 2** was measured in 1,045 liters, the full volume of the cell. Recently, a flow measurement around a breathing and heated human model was performed in a volume of 12 m^3 (Schröder et al. 2022). The use of high-resolution cameras allowed up to 3 million bubbles to be followed instantaneously and small instantaneous turbulent structures of the thermal plume to be resolved, despite the large volume size. Scalable LED illumination has also been applied in water, yielding images free of artifacts caused by coherent light (Kim et al. 2021). The image quality can be further improved by using fluorescent particles and appropriate filters (Kim et al. 2022, Weiss et al. 2022).

A different approach to increasing the volume size was developed by Schneiders et al. (2018) in the form of the coaxial volumetric velocimeter. The measurement device consists of a fixed and precalibrated system of four cameras, installed in a common housing. Between the cameras a volumetric laser illumination is installed (**Figure 8*a***). The light reflected by HFSB seeding is

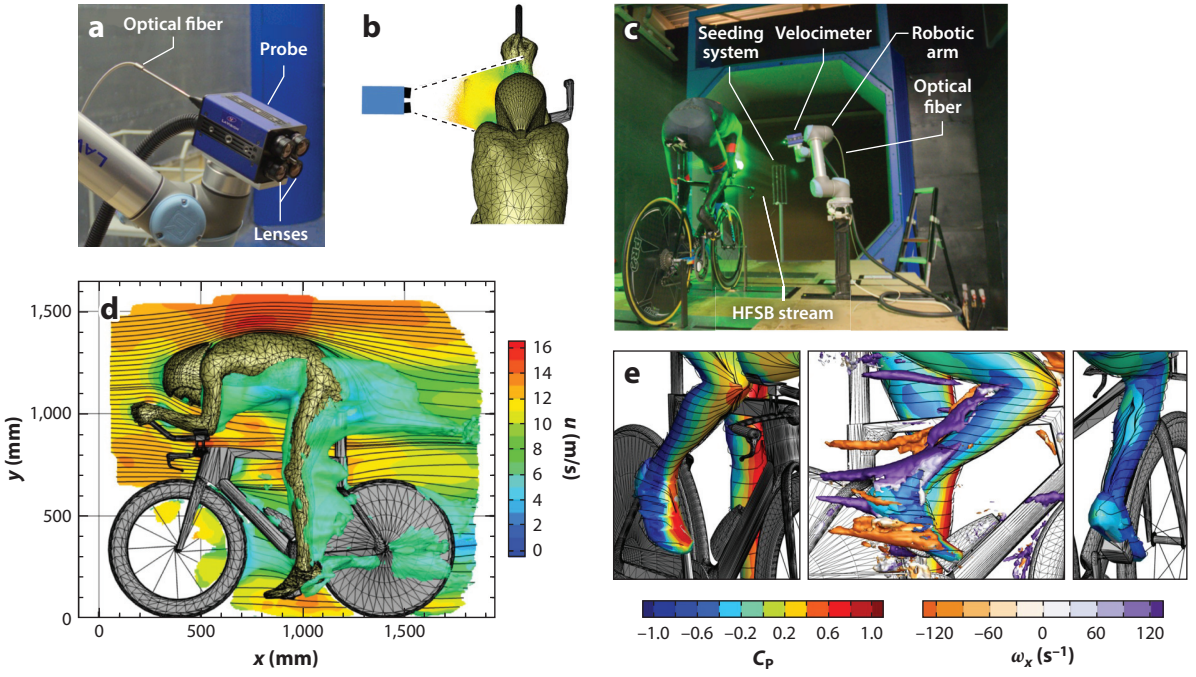

Figure 8

A coaxial volumetric velocimeter for time-averaged large-volumetric measurements. (*a*) Lavision's MiniShaker S consists of a fixed and precalibrated system of four cameras, installed in a common housing. (*b*) Measurement of a single subvolume in front of a cyclist. (*c*) Scanning of the full volume using a robotic arm. (*d*) Time-averaged velocity field around full cyclist model, showing contours of streamwise velocity u in the center plane, together with an isosurface of $u = 7$ m/s. (*e*) Surface pressure coefficient C_P distribution in the foot/ankle region, along with isocontours of the Q-criterion, colored by streamwise vorticity ω_x. Panels *a*, *c*, and *d* adapted from Jux et al. (2018) (CC BY 4.0). Panels *b* and *d* adapted from Jux (2022) with permission; copyright 2021 the author. Abbreviation: HFSB, helium-filled soap bubbles.

recorded by the four cameras; particle trajectories are reconstructed using STB. The device can simply be pointed at a region of interest and operated for a certain time, yielding LPT results in a volume of up to 30 liters (**Figure 8*b***). Larger volumes are scanned by moving the velocimeter on a robotic arm, systematically scanning the object of interest (**Figure 8*c***). One interesting application of the method is the measurement of the flow around a full-scale cyclist (Jux et al. 2018), which yielded the flow in a volume of 2 m^3 at a freestream velocity of 14 m/s by stitching together 450 subvolumes (**Figure 8*d*,*e***). Other examples include an investigation of the flow behind a micro air vehicle (Martínez Gallar et al. 2020) and the determination of all components in Collar's triangle of forces acting on a flexible wing (Mertens et al. 2021). The downsides of the method are the low position accuracy in the depth direction (due to the limited opening angle of the camera views) and the restriction to averaged data due to the scanning approach.

SUMMARY POINTS

1. Lagrangian particle tracking (LPT) can accurately track a large number of particles (10^4–10^6), yielding a high dynamic spatial range (DSR). Applying temporal filtering at calibrated levels yields high dynamic velocity and acceleration ranges (DVRs and DARs).

2. Recent developments in LPT software allow the usable particle image density concentration to be increased by up to ∼0.2 particles per pixel (ppp) using advanced Shake-The-Box (STB) processing—many times more than the densities reached by classical particle tracking velocimetry (PTV) methods. Furthermore, these advances have increased DVR significantly compared to two-pulse tomographic particle image velocimetry (Tomo-PIV) measurements.
3. The dynamics of a flow plays an important role in its evaluation. Regions of quiescent flow can be as problematic for the tracking scheme as rare high-acceleration events or low temporal sampling. The variable space step and variable time step methods improve the tracking performance of the STB scheme in such conditions.
4. High particle densities allow one to create converged single- and multipoint statistics at subpixel resolution (∼0.1 $\overline{\text{px}}$), greatly increasing the DSR for statistical approaches. Statistics for proximities below the diffraction limits of imaging can be reliably determined using functional binning approaches.
5. Time-resolved 3D velocity, acceleration, and pressure fields represented by continuous 3D functions can be determined using novel constrained data assimilation (DA) methods (3D and 4D variational, as well as adjoint). The availability of velocity and acceleration (material derivative) data allows for Navier–Stokes constraints to be used, thereby achieving maximized spatial resolution from the dense scattered tracer particles.
6. The quality of LPT measurements is greatly dependent on the care taken to optimize experimental parameters (e.g., image signal-to-noise ratio, particle scattering properties, available temporal resolution). Likewise, researchers should aim to guarantee a precise calibration at all times using (instantaneous) volume self-calibration. Further correction methods can account for nonlinear effects (e.g., viewing through curved windows).
7. The use of noncoherent light sources (e.g., LED arrays) illuminating sufficiently large tracer particles (e.g., helium-filled soap bubbles in air, polyamide in water) produces particle imaging highly suitable for LPT evaluation in large volumes due to the much-improved superposition and consistency of particle images. Using fluorescent particles additionally minimizes background reflections.

FUTURE ISSUES

1. An enhanced predictor scheme could incorporate corrections using preknowledge of the flow topologies, gained either by computational fluid dynamics (CFD) or previous experimental results. Further improvements are expected using DA of previous time steps, advected to the current time, creating a physics-based space–time link.
2. The effect of particle images overlapping in one or multiple cameras on position accuracy and local bias errors should be quantified. Generally, tools for uncertainty quantification of LPT and DA need to be further developed and assessed.
3. An openly accessible benchmark data set (HOMER LPT and DA Evaluation Portal; **https://w3.onera.fr/flow-benchmarks**) is available and will be extended continuously, allowing researchers for the first time to quantitatively compare different methods on a common synthetic data base using underlying CFD simulations.

4. A further significant increase of processable particle image densities will be difficult to achieve. However, higher particle concentrations (particles per volume) could be reached by using a scanning approach in low-speed flows, avoiding phase shifts by regarding the trajectories as functionals.
5. Current DA approaches mainly apply regularization based on the momentum equation. Further constraints could be gained by using more conservation laws and equations (e.g., the energy equation) and by thoroughly utilizing the temporal resolution.
6. The prediction and correction scheme introduced by the STB method could also be implemented for other 3D flow measurement techniques like holographic, astigmatic, light field, and tomographic particle tracking.

DISCLOSURE STATEMENT

The authors are not aware of any biases that might be perceived as affecting the objectivity of this review.

ACKNOWLEDGMENTS

This work was partly supported by the Deutsche Forschungsgemeinschaft (DFG) through grant SCHR 1165/5-1/2 as part of the Priority Program on Turbulent Superstructures (DFG SPP 1881, first and second period) and the HOMER (Holistic Optical Metrology for Aero-Elastic Research) project from the European Union's Horizon 2020 research and innovation program under grant agreement 769237. The authors thank Matteo Novara and Tobias Jahn for valuable discussions and longstanding support. The help of Philipp Godbersen and Hicham Saaid in the creation of the figures is greatly appreciated.

LITERATURE CITED

Abu Rowin W, Ghaemi S. 2019. Streamwise and spanwise slip over a superhydrophobic surface. *J. Fluid Mech.* 870:1127–57

Adrian RJ. 1997. Dynamic ranges of velocity and spatial resolution of particle image velocimetry. *Meas. Sci. Technol.* 8(12):1393

Adrian RJ, Westerweel J. 2011. *Particle Image Velocimetry*. Cambridge, UK: Cambridge Univ. Press

Agüera N, Cafiero G, Astarita T, Discetti S. 2016. Ensemble 3D-PTV for high resolution turbulent statistics. *Meas. Sci. Technol.* 27:124011

Agüí JC, Jimenez J. 1987. On the performance of particle tracking. *J. Fluid Mech.* 185:447–68

Aguirre-Pablo AA, Aljedaani AB, Xiong J, Idoughi R, Heidrich W, Thoroddsen ST. 2019. Single-camera 3D PTV using particle intensities and structured light. *Exp. Fluids* 60(2):25

Atkinson C, Soria J. 2009. An efficient simultaneous reconstruction technique for tomographic particle image velocimetry. *Exp. Fluids* 47:563–78

Bhattacharya S, Vlachos PP. 2020. Volumetric particle tracking velocimetry (PTV) uncertainty quantification. *Exp. Fluids* 61(9):197

Beresh SJ. 2021. Time-resolved particle image velocimetry. *Meas. Sci. Technol.* 32:102003

Bosbach J, Kühn M, Wagner C. 2009. Large scale particle image velocimetry with helium filled soap bubbles. *Exp. Fluids* 46:539–47

Bosbach J, Schanz D, Godbersen P, Schröder A. 2021. *Spatially and temporally resolved measurements of turbulent Rayleigh-Bénard convection by Lagrangian particle tracking of long-lived helium-filled soap bubbles*. Paper presented at 14th International Symposium on Particle Image Velocimetry, Chicago, Aug. 1–4

Brandt L, Coletti F. 2022. Particle-laden turbulence: progress and perspectives. *Annu. Rev. Fluid Mech.* 54:159–89

Bross M, Fuchs T, Kähler CJ. 2019. Interaction of coherent flow structures in adverse pressure gradient turbulent boundary layers. *J. Fluid Mech.* 873:287–321

Brücker C. 1997. 3D scanning PIV applied to an air flow in a motored engine using digital high-speed video. *Meas. Sci. Technol.* 8:1480

Brunton SL, Noack BR, Koumoutsakos P. 2020. Machine learning for fluid mechanics. *Annu. Rev. Fluid Mech.* 52:477–508

Chiu WC, Rib LN. 1956. The rate of dissipation of energy and the energy spectrum in a low-speed turbulent jet. *Eos* 37(1):13–26

Choi YS, Seo KW, Sohn MH, Lee SJ. 2012. Advances in digital holographic micro-PTV for analyzing microscale flows. *Opt. Lasers Eng.* 50(1):39–45

Chong MS, Perry AE, Cantwell BJ. 1990. A general classification of three-dimensional flow fields. *Phys. Fluids* A2(5):765–77

Cierpka C, Lütke B, Kähler CJ. 2013. Higher order multi-frame particle tracking velocimetry. *Exp. Fluids* 54(5):1533

Cierpka C, Rossi M, Segura R, Kähler CJ. 2010. On the calibration of astigmatism particle tracking velocimetry for microflows. *Meas. Sci. Technol.* 22(1):015401

Cornic P, Leclaire B, Champagnat F, Le Besnerais G, Cheminet A, et al. 2020. Double-frame tomographic PTV at high seeding densities. *Exp. Fluids* 61(2):23

Dabiri D, Pecora C. 2020. *Particle Tracking Velocimetry*. Bristol, UK: IOP

Discetti S, Coletti F. 2018. Volumetric velocimetry for fluid flows. *Meas. Sci. Technol.* 29:042001

Doh DH, Cho GR, Kim YH. 2012. Development of a tomographic PTV. *J. Mech. Sci. Technol.* 26(12):3811–19

Duraisamy K, Iaccarino G, Xiao H. 2019. Turbulence modeling in the age of data. *Annu. Rev. Fluid Mech.* 51:357–77

Ebrahimian M, Sanders RS, Ghaemi S. 2019. Dynamics and wall collision of inertial particles in a solid–liquid turbulent channel flow. *J. Fluid Mech.* 881:872–905

Elsinga GE, Scarano F, Wieneke B, van Oudheusden BW. 2006. Tomographic particle image velocimetry. *Exp. Fluids* 41:933–47

Fahringer TW, Lynch KP, Thurow BS. 2015. Volumetric particle image velocimetry with a single plenoptic camera. *Meas. Sci. Technol.* 26:115201

Fletcher R, Powell M. 1963. A rapidly convergent descent method for minimization. *Comput. J.* 6(2):163–68

Fuchs T, Hain R, Kähler CJ. 2016. Double-frame 3D-PTV using a tomographic predictor. *Exp. Fluids* 57:174

Gao Q, Pan S, Wang H, Wei R, Wang J. 2021. Particle reconstruction of volumetric particle image velocimetry with the strategy of machine learning. *Adv. Aerodyn.* 3:28

Geisler R, Novara M, Schröder A. 2016. *Volumetric multi-pulse particle tracking measurement for separated laminar transitional flow investigations*. Paper presented at 18th International Symposium on Application of Laser and Imaging Techniques to Fluid Mechanics, Lisbon, Port., July 4–7

Gesemann S. 2021. *TrackFit: uncertainty quantification, optimal filtering and interpolation of tracks for time-resolved Lagrangian particle tracking*. Paper presented at 14th International Symposium on Particle Image Velocimetry, Chicago, Aug. 1–4

Gesemann S, Huhn F, Schanz D, Schröder A. 2016. *From noisy particle tracks to velocity, acceleration and pressure fields using B-splines and penalties*. Paper presented at 18th International Symposium on Application of Laser and Imaging Techniques to Fluid Mechanics, Lisbon, Port., July 4–7

Godbersen P, Bosbach J, Schanz D, Schröder A. 2020. *The beauty of turbulent convection: a particle tracking endeavor*. Film presented at Gallery of Fluid Motion, 73rd Annual Meeting of the APS Division of Fluid Dynamics (Virtual), Nov. 22–24

Godbersen P, Bosbach J, Schanz D, Schröder A. 2021. Beauty of turbulent convection: a particle tracking endeavor. *Phys. Rev. Fluids* 6(11):110509

Godbersen P, Schröder A. 2020. Functional binning: improving convergence of Eulerian statistics from Lagrangian particle tracking. *Meas. Sci. Technol.* 31:095304

Godbersen P, Schröder A. 2021. *Enhanced functional binning for one- and two-point statistics using a posteriori Uncertainty Quantification of LPT data*. Paper presented at 14th International Symposium on Particle Image Velocimetry, Chicago, Aug. 1–4

Gray C, Greated CA, McCluskey DR, Easson WJ. 1991. An analysis of the scanning beam PIV illumination system. *Meas. Sci. Techn.* 2:717

Guezennec YG, Brodkey RS, Trigui N, Kent JC. 1994. Algorithms for fully automated three-dimensional particle tracking velocimetry. *Exp. Fluids* 17:209–19

Haller G. 2015. Lagrangian coherent structures. *Annu. Rev. Fluid Mech.* 47:137–62

Hammond A, Meng H. 2021. Particle radial distribution function and relative velocity measurement in turbulence at small particle-pair separations. *J. Fluid Mech.* 921:A16

Herman GT, Lent A. 1976. Iterative reconstruction algorithms. *Comput. Biol. Med.* 6:273–94

Herzog S, Schiepel D, Guido I, Barta R, Wagner C. 2021. A Probabilistic particle tracking framework for guided and Brownian motion systems with high particle densities. *SN Comput. Sci.* 2:485

Hinsch KD. 2002. Holographic particle image velocimetry. *Meas. Sci. Technol.* 13:R61

Hoyer K, Holzner M, Lüthi B, Guala M, Liberzon A, Kinzelbach W. 2005. 3D scanning particle tracking velocimetry. *Exp. Fluids* 39(5):923–34

Huhn F, Schanz D, Gesemann S, Dierksheide U, van de Meerendonk R, Schröder A. 2017. Large-scale volumetric flow measurement in a pure thermal plume by dense tracking of helium-filled soap bubbles. *Exp. Fluids* 58(9):116

Huhn F, Schanz D, Manovski P, Gesemann S, Schröder A. 2018. Time-resolved large-scale volumetric pressure fields of an impinging jet from dense Lagrangian particle tracking. *Exp. Fluids* 59:81

Jahn T, Schanz D, Schröder A. 2021. Advanced iterative particle reconstruction for Lagrangian Particle Tracking. *Exp. Fluids* 62(8):179

Janke T, Michaelis D. 2021. *Uncertainty quantification for PTV/LPT data and adaptive track filtering*. Paper presented at 14th International Symposium on Particle Image Velocimetry, Chicago, Aug. 1–4

Jeon YJ. 2021. *Eulerian time-marching in Vortex-In-Cell (VIC) method: reconstruction of multiple time-steps from a single vorticity volume and time-resolved boundary condition*. Paper presented at 14th International Symposium on Particle Image Velocimetry, Chicago, Aug. 1–4

Jeon YJ, Schneiders JFG, Müller M, Michaelis D, Wieneke B. 2018. *4D flow field reconstruction from particle tracks by VIC+ with additional constraints and multigrid approximation*. Paper presented at 18th International Symposium on Flow Visualization, Zurich, Switz., June 26–29

Jux C. 2022. *Development of robotic volumetric PIV*. PhD Thesis, T.U. Delft, Delft, Neth.

Jux C, Sciacchitano A, Schneiders JF, Scarano F. 2018. Robotic volumetric PIV of a full-scale cyclist. *Exp. Fluids* 59(4):74

Kähler CJ, Astarita T, Vlachos PP, Sakakibara J, Hain R, et al. 2016. Main results of the 4th International PIV Challenge. *Exp. Fluids* 57(6):97

Kähler CJ, Scharnowski S, Cierpka C. 2012. On the uncertainty of digital PIV and PTV near walls. *Exp. Fluids* 52:1641–56

Katz J, Sheng J. 2010. Applications of holography in fluid mechanics and particle dynamics. *Annu. Rev. Fluid Mech.* 42:531–55

Khojasteh AR, Yang Y, Heitz D, Laizet S. 2021. Lagrangian coherent track initialization. *Phys. Fluids* 33(9):095113

Kim D, Schanz D, Novara M, Seo H, Kim Y, et al. 2022. Experimental study of turbulent bubbly jet. Part 1. Simultaneous measurement of three-dimensional velocity fields of bubbles and water. *J. Fluid Mech.* 941:A42

Kim M, Schanz D, Novara M, Schröder A, Kim KC. 2021. *Volumetric Lagrangian particle tracking measurements of jet impingement on convex cylinder*. Paper presented at 14th International Symposium on Particle Image Velocimetry, Chicago, Aug. 1–4

Kozul M, Koothur V, Worth NA, Dawson JR. 2019. A scanning particle tracking velocimetry technique for high-Reynolds number turbulent flows. *Exp. Fluids* 60(8):137

Kühn M, Ehrenfried K, Bosbach J, Wagner C. 2011. Large-scale tomographic particle image velocimetry using helium-filled soap bubbles. *Exp. Fluids* 50:929–48

La Porta A, Voth GA, Crawford AM, Alexander J, Bodenschatz E. 2001. Fluid particle accelerations in fully developed turbulence. *Nature* 409(6823):1017–19

Lasinger K, Vogel C, Pock T, Schindler K. 2020. 3D fluid flow estimation with integrated particle reconstruction. *Int. J. Comput. Vis.* 128(4):1012–27

Lawson JM, Bodenschatz E, Lalescu CC, Wilczek M. 2018. Bias in particle tracking acceleration measurement. *Exp. Fluids* 59(11):172

Lawson JM, Dawson JR. 2014. A scanning PIV method for fine-scale turbulence measurements. *Exp. Fluids* 55(12):1857

Leclaire B, Mary I, Liauzun C, Peron S, Sciacchitano A, et al. 2021. *First challenge on Lagrangian Particle Tracking and Data Assimilation: datasets description and evolution to an open online benchmark*. Paper presented at 14th International Symposium on Particle Image Velocimetry, Chicago, Aug. 1–4

Lüthi B, Tsinober A, Kinzelbach W. 2005. Lagrangian measurement of vorticity dynamics in turbulent flow. *J. Fluid Mech.* 528:87–118

Lynch KP, Scarano F. 2014. Material acceleration estimation by four-pulse tomo-PIV. *Meas. Sci. Technol.* 25(8):084005

Lynch KP, Scarano F. 2015. An efficient and accurate approach to MTE-MART for time-resolved tomographic PIV. *Exp. Fluids* 56:66

Lynch KP, Wagner JL. 2022. Pulse-burst tomographic PIV of an impulsively started cylinder wake in a shock tube. *Exp. Fluids* 63:51

Maas HG, Gruen A, Papantoniou D. 1993. Particle tracking velocimetry in three-dimensional flows. Part I: photogrammetric determination of particle coordinates. *Exp. Fluids* 15:133–46

Machicoane N, Huck PD, Clark A, Aliseda A, Volk R, Bourgoin M. 2019. Recent developments in particle tracking diagnostics for turbulence research. In *Flowing Matter*, ed. F Toschi, M Sega, pp. 177–209. Cham, Switz.: Springer

Malik N, Dracos T, Papantoniou D. 1993. Particle tracking velocimetry in three dimensional flows. Part II: particle tracking. *Exp. Fluids* 15:279–94

Mani M, Dorgan AJ. 2023. A perspective on the state of aerospace computational fluid dynamics technology. *Annu. Rev. Fluid Mech.* 55:431–57

Manovski P, Novara M, Mohan NKD, Geisler R, Schanz D, et al. 2021. 3D Lagrangian particle tracking of a subsonic jet using multi-pulse Shake-The-Box. *Exp. Therm. Fluid Sci.* 123:110346

Martínez Gallar B, van Oudheusden BW, Sciacchitano A, Karásek M. 2020. Large-scale volumetric flow visualization of the unsteady wake of a flapping-wing micro air vehicle. *Exp. Fluids* 61:16

Mendez MA, Raiola M, Masullo A, Discetti S, Ianiro A, et al. 2017. POD-based background removal for particle image velocimetry. *Exp. Therm. Fluid Sci.* 80:181–92

Mertens C, de Rojas Cordero T, Sodja J, Sciacchitano A, van Oudheusden BW. 2021. Aeroelastic characterization of a flexible wing using particle tracking velocimetry measurements. *AIAA J.* 60(1):276–86

Michaelis D, Novara M, Scarano F, Wieneke B. 2010. *Comparison of volume reconstruction techniques at different particle densities*. Paper presented at 15th International Symposium on Application of Laser and Imaging Techniques to Fluid Mechanics, Lisbon, Port., July 5–8

Michaelis D, Wiswall J, Mychkovsky A, Prevost R, Neal D, Wieneke B. 2021. *Calibration correction of arbitrary optical distortions by non-parametric 3D disparity field for planar and volumetric PIV/LPT*. Paper presented at 14th International Symposium on Particle Image Velocimetry, Chicago, Aug. 1–4

Nayler JL, Frazer BA. 1917. *Preliminary report upon an experimental method of investigating, by the aid of kinematographic photography, the history of eddying flow past a model immersed in water*. Tech. Rep., Adv. Comm. Aeronaut., London

Nishino K, Kasagi N, Hirata M. 1989. Three-dimensional particle tracking velocimetry based on automated digital image processing. *Trans ASME J. Fluid Eng.* 111:384–90

Nocedal J. 1980. Updating quasi-Newton matrices with limited storage. *Math. Comput.* 35:773–82

Novara M, Batenburg KJ, Scarano F. 2010. Motion tracking enhanced MART for tomographic PIV. *Meas. Sci. Technol.* 21:035401

Novara M, Scarano F. 2013. A particle-tracking approach for accurate material derivative measurements with tomographic PIV. *Exp. Fluids* 54:1584

Novara M, Schanz D, Geisler R, Gesemann S, Voss C, Schröder A. 2019. Multi-exposed recordings for 3D Lagrangian particle tracking with multi-pulse Shake-The-Box. *Exp. Fluids* 60(3):44

Novara M, Schanz D, Gesemann S, Lynch KP, Schröder A. 2016a. *Lagrangian 3D particle tracking for multi-pulse systems: performance assessment and application of Shake-The-Box*. Paper presented at 18th International

Symposium on Application of Laser and Imaging Techniques to Fluid Mechanics, Lisbon, Portugal, July 4–7

Novara M, Schanz D, Reuther N, Kähler CJ, Schröder A. 2016b. Lagrangian 3D particle tracking in high-speed flows: Shake-The-Box for multi-pulse systems. *Exp. Fluids* 57:128

Novara M, Schanz D, Schröder A. 2022. *Two-pulse 3D particle tracking with Shake-The-Box*. Paper presented at 20th International Symposium on Application of Laser and Imaging Techniques to Fluid Mechanics, Lisbon, Portugal, July 11–14

Ouellette NT, Xu H, Bodenschatz E. 2006. A quantitative study of three-dimensional Lagrangian particle tracking algorithms. *Exp. Fluids* 40:301–13

Pereira F, Gharib M, Dabiri D, Modarress D. 2000. Defocusing digital particle image velocimetry: a 3-component 3-dimensional DPIV measurement technique. Application to bubbly flows. *Exp. Fluids* 29:S078–84

Raffel M, Willert CE, Scarano F, Kähler CJ, Wereley ST, Kompenhans J. 2018. *Particle Image Velocimetry: A Practical Guide*. Cham, Switz.: Springer. 3rd ed.

Raiola M, Lopez-Nuñez E, Cafiero G, Discetti S. 2020. Adaptive ensemble PTV. *Meas. Sci. Technol.* 31(8):085301

Richardson LF. 1922. *Weather Prediction by Numerical Process*. Cambridge, UK: Cambridge Univ. Press

Rival DE, van Oudheusden B. 2017. Load-estimation techniques for unsteady incompressible flows. *Exp. Fluids* 58(3):20

Savitzky A, Golay MJE. 1964. Smoothing and differentiation of data by simplified least squares procedures. *Anal. Chem.* 36(8):1627–39

Scarano F. 2013. Tomographic PIV: principles and practice. *Meas. Sci. Technol.* 24:012001

Scarano F, Ghaemi S, Caridi GCA, Bosbach J, Dierksheide U, Sciacchitano A. 2015. On the use of helium-filled soap bubbles for large-scale tomographic PIV in wind tunnel experiments. *Exp. Fluids* 56:42

Scarano F, Schneiders JF, Saiz GG, Sciacchitano A. 2022. Dense velocity reconstruction with VIC-based time-segment assimilation. *Exp. Fluids* 63(6):96

Schanz D, Gesemann S, Schröder A. 2016. Shake-The-Box: Lagrangian particle tracking at high particle image densities. *Exp. Fluids* 57:570

Schanz D, Gesemann S, Schröder A, Wieneke B, Novara M. 2013a. Non-uniform optical transfer functions in particle imaging: calibration and application to tomographic reconstruction. *Meas. Sci. Technol.* 24:024009

Schanz D, Jahn T, Schröder A. 2022. *3D particle position determination and correction at high particle densities*. Paper presented at 20th International Symposium on Application of Laser and Imaging Techniques to Fluid Mechanics, Lisbon, Portugal, July 11–14

Schanz D, Novara M, Schröder A. 2021. *Shake-The-Box particle tracking with variable time-steps in flows with high velocity range (VT-STB)*. Paper presented at 14th International Symposium on Particle Image Velocimetry, Chicago, Aug. 1–4

Schanz D, Schröder A, Gesemann S, Michaelis D, Wieneke B. 2013b. *Shake-The-Box: a highly efficient and accurate Tomographic Particle Tracking Velocimetry (TOMO-PTV) method using prediction of particle position*. Paper presented at 10th International Symposium on Particle Image Velocimetry, Delft, Neth., July 1–3

Schanz D, Schröder A, Novara M, Geisler R, Agocs J, et al. 2019. *Large-scale volumetric characterization of a turbulent boundary layer flow*. Paper presented at 13th International Symposium on Particle Image Velocimetry, Munich, Ger., July 22–24

Schneiders JFG, Scarano F. 2016. Dense velocity reconstruction from tomographic PTV with material derivatives. *Exp. Fluids* 57:139

Schneiders JFG, Scarano F, Jux C, Sciacchitano A. 2018. Coaxial volumetric velocimetry. *Meas. Sci. Technol.* 29(6):065201

Schneiders JFG, Sciacchitano A. 2017. Track benchmarking method for uncertainty quantification of particle tracking velocimetry interpolations. *Meas. Sci. Technol.* 28:065302

Schröder A, Geisler R, Staak K, Wieneke B, Elsinga G, et al. 2011. Eulerian and Lagrangian views into a turbulent boundary layer flow using time-resolved tomographic PIV. *Exp. Fluids* 50:1071–91

Schröder A, Schanz D, Bosbach J, Novara M, Geisler R, et al. 2022. Large-scale volumetric flow studies on transport of aerosol particles using a breathing human model with and without face protections. *Phys. Fluids* 34:035133

Schröder A, Schanz D, Geisler R, Willert C, Michaelis D. 2013. *Dual-volume and four-pulse tomo PIV using polarized laser lights.* Paper presented at 10th International Symposium on Particle Image Velocimetry, Delft, Neth., July 1–3

Schröder A, Schanz D, Gesemann S, Huhn F, Buchwald T, et al. 2022. *Measurements of the energy dissipation rate in homogeneous turbulence using dense 3D Lagrangian Particle Tracking and FlowFit.* Paper presented at 20th International Symposium on Application of Laser and Imaging Techniques to Fluid Mechanics, Lisbon, Portugal, July 11–14

Schröder A, Schanz D, Michaelis D, Cierpka C, Scharnowski S, Kähler CJ. 2015. Advances of PIV and 4D-PTV "Shake-The-Box" for turbulent flow analysis—the flow over periodic hills. *Flow Turbul. Combust.* 95(2):193–209

Schröder A, Willert C, eds. 2008. *Particle Image Velocimetry: New Developments and Recent Applications*. Top. Appl. Phys. 112. Berlin: Springer-Verlag

Schröder A, Willert C, Schanz D, Geisler R, Jahn T, et al. 2020. The flow around a surface mounted cube: a characterization by time-resolved PIV, 3D Shake-The-Box and LBM simulation. *Exp. Fluids* 61:189

Sciacchitano A, Leclaire B, Schröder A. 2021a. *Main results of the first data assimilation challenge*. Paper presented at 14th International Symposium on Particle Image Velocimetry, Chicago, Aug. 1–4

Sciacchitano A, Leclaire B, Schröder A. 2021b. *Main results of the first Lagrangian particle tracking challenge*. Paper presented at 14th International Symposium on Particle Image Velocimetry, Chicago, Aug. 1–4

Shnapp R, Shapira E, Peri D, Bohbot-Raviv Y, Fattal E, Liberzon A. 2019. Extended 3D-PTV for direct measurements of Lagrangian statistics of canopy turbulence in a wind tunnel. *Sci. Rep*. 9:7405

Sellappan P, Alvi FS, Cattafesta LN. 2020. Lagrangian and Eulerian measurements in high-speed jets using Multi-Pulse Shake-The-Box and fine scale reconstruction (VIC#). *Exp. Fluids* 61:157

Stasicki B, Schröder A, Boden F, Ludwikowski K. 2017. High-power LED light sources for optical measurement systems operated in continuous and overdriven pulsed modes. In *Optical Measurement Systems for Industrial Inspection X*, Vol. 10329, ed. P Lehmann, W Osten, AA Gonçalves Jr., Pap. 103292J. Bellingham, WA: SPIE

Tan S, Salibindla A, Masuk AUM, Ni R. 2020. Introducing OpenLPT: new method of removing ghost particles and high-concentration particle shadow tracking. *Exp. Fluids* 61(2):47

Toschi F, Bodenschatz E. 2009. Lagrangian properties of particles in turbulence. *Annu. Rev. Fluid Mech.* 41:375–404

van Gent PL, Michaelis D, van Oudheusden BW, Weiss PÉ, De Kat R, et al. 2017. Comparative assessment of pressure field reconstructions from PIV measurements and Lagrangian particle tracking. *Exp. Fluids* 58:33

Viggiano B, Basset T, Solovitz S, Barois T, Gibert M, et al. 2021. Lagrangian diffusion properties of a free shear turbulent jet. *J. Fluid Mech.* 918:A25

Virant M, Dracos T. 1997. 3D PTV and its application on Lagrangian motion. *Meas. Sci. Technol.* 8:1539

Wang L, Pan C, Liu J, Cai C. 2020. Ratio-cut background removal method and its application in near-wall PTV measurement of a turbulent boundary layer. *Meas. Sci. Technol.* 32(2):025302

Weiss S, Schanz D, Erdogdu AO, Schröder A, Bosbach J. 2022. *Investigation of turbulent superstructures in Rayleigh-Benard convection by Lagrangian particle tracking of fluorescent microspheres*. Paper presented at 20th International Symposium on Application of Laser and Imaging Techniques to Fluid Mechanics, Lisbon, Portugal, July 11–14

Westerweel J, Elsinga GE, Adrian RJ. 2013. Particle image velocimetry for complex and turbulent flows. *Annu. Rev. Fluid Mech.* 45:409–36

Wieneke B. 2008. Volume self-calibration for 3D particle image velocimetry. *Exp. Fluids* 45:549–56

Wieneke B. 2012. Iterative reconstruction of volumetric particle distribution. *Meas. Sci. Technol.* 24:024008

Wieneke B. 2018. Improvements for volume self-calibration. *Meas. Sci. Technol.* 29(8):084002

Wiener N. 1949. *Extrapolation, Interpolation, and Smoothing of Stationary Time Series*, Vol. 2. Cambridge, MA: MIT Press

Willert CE, Gharib M. 1992. Three-dimensional particle imaging with a single camera. *Exp. Fluids* 12(6):353–58

Xu H. 2008. Tracking Lagrangian trajectories in position–velocity space. *Meas. Sci. Technol.* 19:075105

Yang Y, Heitz D. 2021. Kernelized Lagrangian particle tracking. *Exp. Fluids* 62(12):252

Annual Review of Fluid Mechanics

Volume 55, 2023

Contents

Indexes

Errata

An online log of corrections to *Annual Review of Fluid Mechanics* articles may be found at http://www.annualreviews.org/errata/fluid